Journal of Statistical Physics, Vol. 48, Nos. 1/2, 1987

Homoclinic Orbits and Mixed-Mode Oscillations in Far-from-Equilibrium Systems

P. Gaspard[1] and X.-J. Wang[1]

Received July 16, 1986; revision received January 6, 1987

Nonlinear autonomous dynamical systems with a *homoclinic tangency to a periodic orbit* are investigated. We study the bifurcation sequences of the mixed-mode oscillations generated by the homoclinicity, which are shown to belong to two different types, depending on the nature of the Liapunov numbers of the basic periodic orbit. A detailed numerical analysis is carried out to show how the existence of a tangent homoclinic orbit allows us to understand in a quantitative way a particular and regular sequence of cool flame-ignition oscillations observed in a thermokinetic model of hydrocarbon oxidation. Chaotic cool flame oscillations are also observed in the same model. When the control parameter crosses a critical value, this chaotic set of trajectories becomes globally unstable and forms a Cantor-like hyperbolic repellor, and the ignition mechanism generates a *homoclinic tangency to the Cantor set of trajectories.* The complex bifurcation diagram may be globally reconstructed from a one-dimensional dynamical system, thanks to the strong contractivity of thermokinetics. It is found that a symbolic dynamics with three symbols is necessary to classify the periodic windows of the complex bifurcation sequence observed numerically in this system.

KEY WORDS: Homoclinic tangency; bifurcation theory; periodic attractors; chaos; hyperbolic repellor; symbolic dynamics; chemical thermokinetics; cool flame-ignition oscillations.

1. INTRODUCTION

Recent advances in the study of the time evolution of chemical systems far from equilibrium reveal the existence of complex dynamical behaviors such as bifurcation sequences of mixed-mode oscillations as well as chaotic behaviors which are *intrinsic* to the system and arise from the nonlinear character of the kinetics.[1-7]

[1] Faculté des Sciences, Université Libre de Bruxelles, B-1050 Brussels, Belgium.

0022-4715/87/0700-0151$05.00/0

Many classes of chemical reactions and, in particular, those involved in combustion present a very complex kinetics with a multitude of intermediate steps having an autocatalytic character. Moreover, time scales ranging from 10^{-6} to 10^{3} sec are commonly realized in laboratory experiments. It is remarkable that, despite the considerable diversity of macroscopic dynamical regimes presented by a chemical system far from equilibrium, the bifurcation pattern of these nonequilibrium behaviors can be modeled by suitably parametrized nonlinear dynamical systems involving a small number of variables. For instance, one-dimensional mappings on the interval have been shown by Simoyi *et al.* to account for the U-sequence experimentally observed in the Belousov–Zhabotinskii (BZ) reaction.[8] Similarly, Pikovsky has accounted for the alternated periodic–chaotic sequence in the BZ reaction, using a one-dimensional map.[9]

Despite the great interest of such discoveries, it is desirable to establish whenever possible a close connection between the abstract mathematical model giving rise to the observed bifurcation sequence and the underlying (continuous-time) flow describing the kinetics of the real-world system. The investigation of complex bifurcations based on such a connection for a class of kinetic mechanism of relevance in both the BZ reaction and in combustion is the principal goal of the present work.

As it will turn out, the dynamical systems relevant for these purposes are systems possessing a *tangent homoclinic orbit*. This class enables one to comprehend in a very general way one type of universal behavior arising in chemical reactions out of equilibrium, namely regular bifurcation sequences of mixed-mode oscillations. This behavior occurs in several systems, such as the BZ reaction,[2,4] heterogeneous catalysis,[10] and combustion.[6,7]

A homoclinic system displays in phase space a bounded domain containing a fixed point, a periodic orbit, or even a more complex invariant set, such as a torus or a quasirandom set of trajectories (see Fig. 1). In each case, the invariant set must be of the saddle type, so that trajectories may reach the neighborhood of the basic invariant set along the stable manifold, stay there for a certain time, and escape along the unstable manifold. A second important property of homoclinic systems is that the flow must *reinject* the outgoing trajectories back into the invariant set. This will be the case if there exists a *homoclinic orbit* associated to the invariant set, i.e., an orbit converging to this latter in both the past and the future. Such a scheme was called *principle of reinjection* by Rössler,[11,12] who showed how a reinjection may induce complex dynamical behaviors. As stressed previously, homoclinic orbits are at the origin of chaotic behaviors.[13–15] In addition, they generate highly regular bifurcation sequences of mixed-mode oscillations.[16,17] We believe that a reinjection scheme is likely to play an

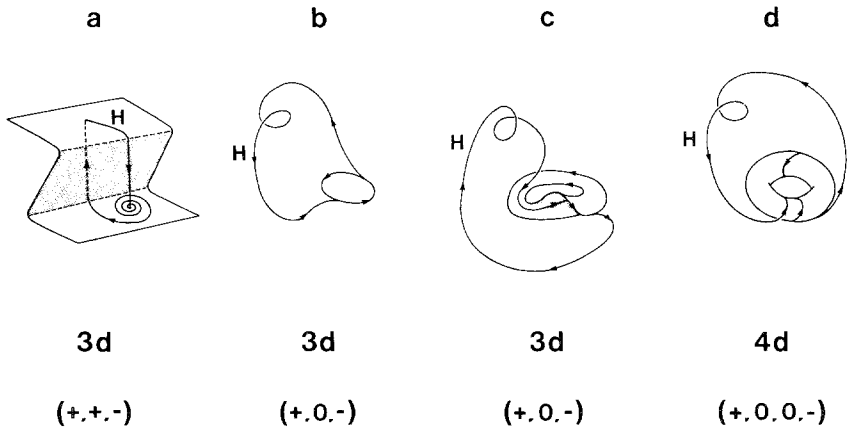

Fig. 1. Various types of homoclinicity: (a) to a saddle fixed point; (b) to a periodic orbit; (c) to a quasirandom invariant set, such as a Smale horseshoe; (d) to a torus. The dimension of the phase space of the dynamical system of the lowest possible dimension and the stability spectrum of the basic invariant set are written down.

important role in chemical kinetics because of the different time scales that may be involved in the reaction steps. If the system starts near a fixed point or a periodic orbit, one variable may slowly drift up to a critical value where a rapid jump may occur. The hyperbolic character of the basic invariant set and the existence of a homoclinic loop are clearly essential in this scheme. As a matter of fact, recent experiments by Argoul *et al.*[19] provide strong evidence of the role of homoclinic orbits in the dynamics of the BZ reaction.

In Sections 2–4 we study the homoclinic orbit associated to a *periodic orbit* (or cycle) in three variable dynamical systems, thus extending previous investigations on homoclinic orbits associated to a fixed point.[15,17] By assumption, the basic cycle is of the saddle type, so that two invariant surfaces, the stable and unstable manifolds, emanate from the basic cycle in the phase space, as shown in Fig. 2. The former (resp. the latter) contains all the trajectories converging to the cycle in the future (resp. the past). Both manifolds intersect along a trajectory called a *homoclinic orbit*. Such an orbit converges to the basic cycle in the past and the future because it belongs to the stable and the unstable manifolds.

Typically, the intersection of both manifolds is transverse. As a result, the homoclinic orbit is structurally stable, i.e., it deforms continuously without disappearing as the control parameter μ of the flow is changed, as shown in Fig. 3a.

Clearly, such a homoclinic orbit cannot generate bifurcation phenomena until a supplementary condition is fulfilled, namely that the

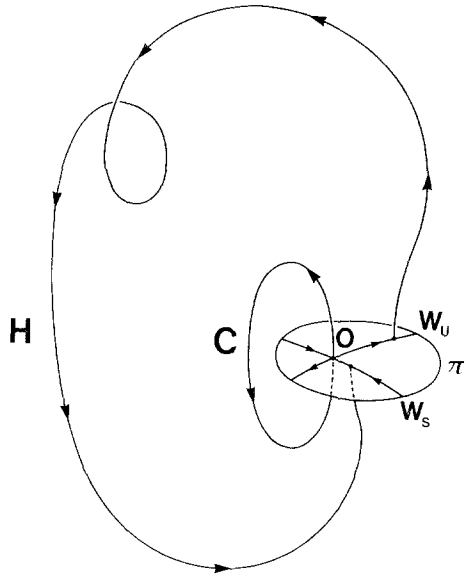

Fig. 2. Geometry of the basic periodic orbit C, its stable and unstable manifolds W_s and W_u, one homoclinic orbit H, and the plane of section π in the phase space. O is the intersection of C with π.

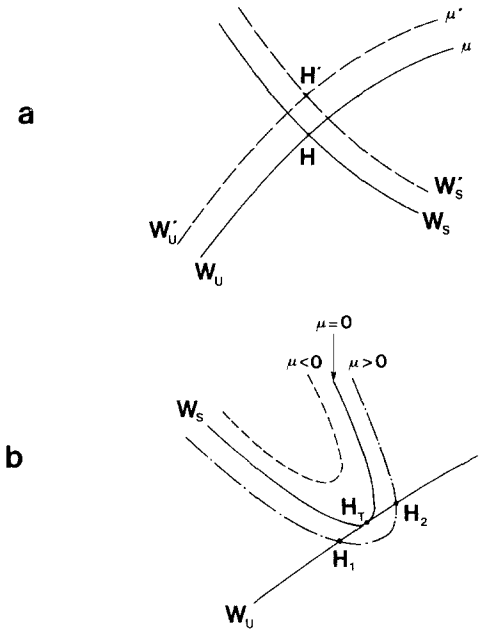

Fig. 3. (a) Homoclinic intersection H of the stable W_s and unstable W_u manifolds for two parameter values (—) μ and (- -) μ'. (b) Homoclinic tangency at H_T of both manifolds. When μ decreases, homoclinic orbits H_1 and H_2 coalesce at $\mu=0$ and disappear when $\mu<0$.

stable manifold becomes tangent to the unstable one at a critical parameter value chosen for convenience to be $\mu = 0$. Such a configuration is called a *homoclinic tangency* to a periodic orbit (see Fig. 3b). A homoclinic tangency is structurally unstable because a small perturbation of the parameter destroys it. Systems with homoclinic tangency are thus codimension 1 systems, since they occupy a surface of dimension $p-1$ in a p-dimensional parameter space.[2]

Another mechanism leading to complex dynamical behaviors such as chaos and based also on a reinjection principle is the intermittency of Pomeau and Manneville.[21] The critical intermittent systems are also codimension 1 systems with a reinjection loop associated to a limit cycle. Here, however, the basic cycle is at a critical situation of codimension 1 bifurcation with some Liapunov numbers on the unit circle and the reinjection is arbitrary. On the contrary, in the systems with a homoclinic tangency associated to a cycle, it is the reinjection mapping that is of codimension 1, because it produces the tangency between the stable and the unstable manifolds, while the Liapunov numbers of the basic cycle remain away from the unit circle. As a consequence of the marginality of the basic cycle in the intermittent systems, the trajectories leave the cycle as $1/t^{\nu}$ for $t \to -\infty$ (with $\nu = 1$ for type I intermittency, $\nu = 1/2$ for type II, and $\nu = 1/2$ or 1 for type III), while the escape from the cycle in systems with a homoclinic tangency behaves like $e^{\alpha t}$ for $t \to -\infty$ (with $\alpha > 0$).

In Section 2, we review analytic results on bifurcation sequences near a homoclinic tangency to a basic cycle. The type of the bifurcation sequence is shown to depend strongly on the stability properties of the basic cycle.

In Sections 3 and 4, a homoclinic tangency to a periodic orbit is revealed in chemical kinetics by a detailed analysis of mixed-mode oscillations in a thermokinetic model. The importance of this model lies in the fact that it is three-dimensional, which is the minimal dimension where complex dynamics such as chaotic behaviors are possible. Nevertheless, this model is realistic because it is bimolecular, obeys the principles of chemical kinetics, and contains qualitatively all the behaviors observed in current experiments on gaseous-phase hydrocarbon oxidation.[6,7] In particular, the model describes not only the cool flame oscillations with small temperature variations, but also the ignition oscillations, which reach higher temperatures. Mixed-mode oscillations where cool flame peaks are mixed with ignition peaks are present in the model and they will indeed be a focus of attention in this paper.

[2] The homoclinic orbit associated to a fixed point of the saddle type in three-variable systems is structurally unstable, so that we may also regard these systems as presenting a homoclinic tangency. In fact, in these systems, the two-dimensional unstable (resp. stable) manifold literally contains the one-dimensional stable (resp. unstable) one.

Systems with homoclinic orbits to a Shil'nikov saddle focus or a basic cycle are known to have an invariant set which is a Cantor set of trajectories whose dynamics is in correspondence with a symbolic dynamics.[14,20,22] Tangency between the stable and unstable manifolds of an invariant set of Cantor type may occur, as remarked by Newhouse in this context.[23,33] In such a scheme, a first homoclinic tangency to a fixed point or a basic cycle generates a Cantor-like invariant set, which sustains in turn secondary homoclinic tangencies.

Nevertheless, the invariant set of Cantor type may be a simple Smale horseshoe[24] originating from a scenario different from the first homoclinic tangency, for instance, a simple Feigenbaum period doubling cascade. If a reinjection mechanism exists in the system, the unstable manifolds of this Smale horseshoe may still have tangencies with its stable manifolds. These features distinguish our scenario at the origin of a homoclinic tangency to a Cantor set of trajectories from the previously investigated scenario.[23,33]

In Section 5, we show how such a homoclinic tangency to a Cantor-like invariant set occurs in the thermokinetic model. The Smale horseshoe is generated only from the cool flame oscillations. As the thermokinetic reinjection mechanism in the ignition regime is strongly contractive, the periodic attractors with mixed ignition and cool flame peaks born via the homoclinic reinjection are very abundant and dominate the time behaviors. Chaotic behaviors with ignition become unobservable numerically even at the high precision we used. Thus, the most interesting behavior of the system is the complex bifurcation sequence of mixed-mode periodic attractors. In Section 5, we give the theoretical elements for a global understanding (up to a given precision) of the pattern of complex bifurcations observed in the model.

In Section 6, the conditions of existence of the mixed-mode oscillations with respect to chaotic behaviors predicted by the theory are compared. Some conclusions on modeling of complex oscillations in thermokinetics are drawn.

2. HOMOCLINIC TANGENCY TO A PERIODIC ORBIT: GENERAL RESULTS

Homoclinic tangencies to a periodic solution in autonomous or periodically forced differential equation systems have been studied by several authors.[22,33,34] In particular, it is known that these systems possess a quasirandom subdynamics, as proved by Gavrilov and Shil'nikov.[22] Furthermore, Newhouse showed that systems with infinitely many sinks exist near homoclinic tangencies.[33,34,41] These fundamental results have generated much interest in view of the understanding of strange attractors.

In the present paper, we shall consider only the simplest periodic attractors, which are generated near the homoclinic tangency. As explained in the introduction, in concrete physicochemical systems, the flow may be so contractive that the chaotic behaviors disappear. The simplest periodic attractors are then dominating and undergo nontrivial bifurcations. Such a phenomenon is more likely to occur in autonomous systems than in periodically forced systems, because these latter systems are equivalent to a single two-dimensional (2D) mapping, whereas several successive 2D mappings of wildly different contractivities could be necessary to understand a 3D flow.

To appreciate better the effect of flow contraction on the bifurcation diagram of periodic attractors, we shall first construct them in the case where the flow is regular, i.e., not specially contractive, and next in the limiting case where the flow along the homoclinic loop is infinitely contracting.

2.1. The Flow Contains a Regular Homoclinic Mapping

Let the 3D differential equation system

$$\dot{\mathbf{X}} = \mathbf{F}_\mu(\mathbf{X}) \tag{2.1}$$

possess, at $\mu = 0$, a homoclinic tangency to a periodic orbit C of period τ_C and of eigenvalues λ_u, λ_s satisfying[3]

$$|\lambda_s| < 1 < |\lambda_u| < 1/|\lambda_s| \tag{2.2}$$

It is well known[22,34,40] that solutions with period increasing like $n\tau_C$ are generated in successive saddle-node bifurcations at critical parameter values $(\mu)'_n$ accumulating like

$$\lim_{n \to \infty} \frac{(\mu)'_{n+1} - (\mu)'_n}{(\mu)'_n - (\mu)'_{n-1}} = \frac{1}{\lambda_u} \tag{2.3}$$

at the homoclinic tangency $\mu = 0$. Between each saddle-node bifurcation and a following period doubling, there exists a periodic attractor.

Since the flow preserves the orientation in the phase space $\mathbb{R}^3$, either

$$\lambda_s, \lambda_u > 0 \qquad \text{(type I)} \tag{2.4}$$

or

$$\lambda_s, \lambda_u < 0 \qquad \text{(type II)} \tag{2.5}$$

[3] A system with $|\lambda'_s \lambda'_u| > 1$ can always be transformed into a system satisfying these conditions by reversing the time $t \to -t$: $\lambda_s = 1/\lambda'_u$, $\lambda_u = 1/\lambda'_s$.

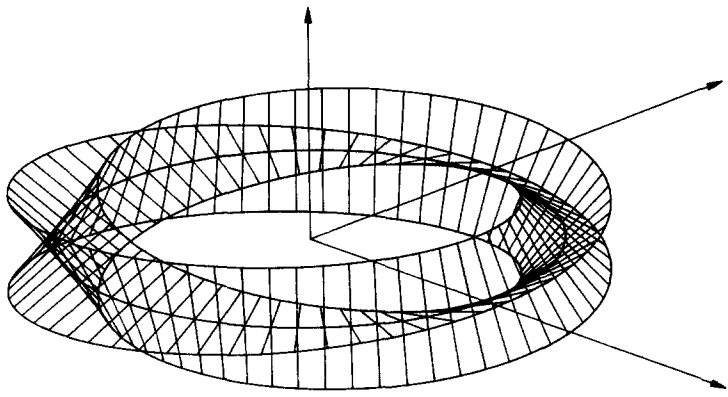

Fig. 4. The invariant stable and unstable manifolds of a periodic orbit of type II with λ_u, $\lambda_s < 0$ form Möbius strips.

In the type I, all the periodic windows occur on the same side of the homoclinic tangency. In the type II, when the invariant manifolds form Möbius strips (see Fig. 4), all the windows of even period lie on one side and all those of odd period on the other side.

In higher dimensional phase space, the constraints from the preservation of the orientation are less restrictive, so that all the different combinations of signs for λ_{s1} and λ_{u1}, the stable and unstable eigenvalues the closest to the unit circle, are possible.

Our purpose here is to construct the bifurcation diagrams of these periodic windows born at parameter values $(\mu)_n^t$ to be compared with the bifurcation diagrams of the thermokinetic model constructed numerically in the next sections.

Let us consider a Poincaré section plane π transverse to the basic periodic orbit C as shown in Fig. 2. By Sternberg's linearization theorem,[35] the curvilinear coordinates can be chosen in the section plane so that the map $\mathbf{T}_0$ induced by the flow near the cycle C is linear and that the stable and unstable manifolds lie on the x axis and the y axis, respectively, as shown in Fig. 5. The definition domain σ_0 of $\mathbf{T}_0$ is restricted to a small neighborhood around C,

$$\mathbf{T}_0 : \sigma_0 \to \sigma_0' \begin{cases} x_0' = \lambda_s(\mu)\, x_0 & (2.6) \\ y_0' = \lambda_u(\mu)\, y_0 & (2.7) \\ t_0' = t_0 + \tau_0(x_0, y_0; \mu) & (2.8) \end{cases}$$

Equation (2.8) governs the return times in the section plane. If the point

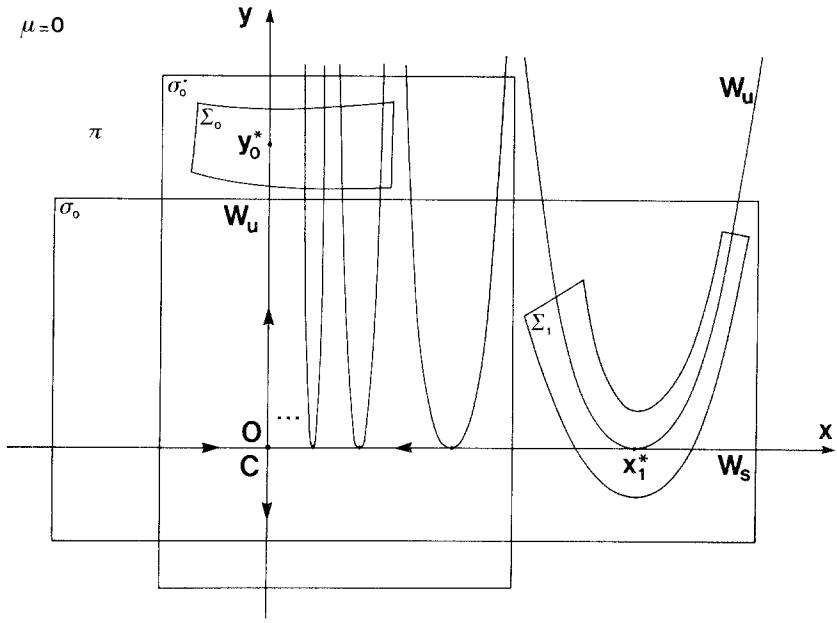

Fig. 5. Geometry of the stable and unstable manifolds in the neighborhood of the basic periodic orbit C in the section plane π at the homoclinic tangency $\mu = 0$ in the case $\lambda_s, \lambda_u > 0$. Here σ_0 (resp. σ_0') is the definition (resp. range) domain of the map $\mathbf{T}_0$; Σ_0 (resp. Σ_1) is the definition (resp. range) domain of $\mathbf{T}_1$; and x_1^* is the intersection point of the tangent homoclinic orbit in Σ_1, with y_0^* that in Σ_0.

(x_0, y_0) is near the periodic orbit, the return time is close to the period, so that to simplify we assume that

$$\tau_0(x_0, y_0; \mu) = \tau_C(\mu) \tag{2.9}$$

The homoclinic tangency produces the geometry of the stable and unstable manifolds of C depicted in Fig. 5. When $\mu = 0$, the tangent homoclinic orbit crosses the section plane at the point $(0, y_0^*)$ on the local unstable manifold W_u and at the point $(x_1^*, 0)$ on the local stable manifold W_s, where the tangency with the global unstable manifold is displayed. A map $\mathbf{T}_1$ is thus induced by the flow from a vicinity Σ_0 of W_u to a vicinity Σ_1 of W_s, which models the reinjection mechanism to the basic cycle C.

A map $\mathbf{T}_1$ capturing these features can be cast into the form

$$\mathbf{T}_1 : \Sigma_0 \to \Sigma_1 \begin{cases} x_1 = x_1^*(\mu) - a(\mu)[y_0 - y_0^*(\mu)] & (2.10) \\ y_1 = b(\mu)\,\mu + c(\mu)\,x_0 + \tfrac{1}{2}d(\mu)[y_0 - y_0^*(\mu)]^2 & (2.11) \\ t_1 = t_0 + \tau_1(x_0, y_0; \mu) & (2.12) \end{cases}$$

The quadratic term in (2.11) reproduces a generic quadratic tangency in agreement with the given geometry. The term in $(y_0 - y_0^*)$ is absent from (2.11) because the tangency is required at $\mu = 0$. The term linear in x_0 is not essential in (2.10) because it leads only to shear distortion parallel to the unstable manifold in Σ_1. The higher order terms are unessential.

Two structurally stable homoclinic orbits exist when $b\mu/d < 0$. They coalesce at the tangency $\mu = 0$ to disappear when $b\mu/d > 0$ (cf. Fig. 3b).

In an analytic system (2.1), such an invertible representation of the map $\mathbf{T}_1$ is possible only in a small neighborhood around the tangent homoclinic orbit. Away from Σ_0, the nonlinearity of the flow may deform considerably the shape of the invariant manifolds. Since $\mathbf{T}_1$ is orientation-preserving in the phase space $\mathbb{R}^3$, its Jacobian satisfies

$$\partial(x_1, y_1)/\partial(x_0, y_0) = ac > 0 \tag{2.13}$$

The function τ_1 is the return time in the plane π during the map $\mathbf{T}_1$ and depends in general on the initial conditions in autonomous systems. We shall choose here a function linear in the coordinates

$$\tau_1(x_0, y_0) = \tau_{1H} + t_{1x} x_0 + t_{1y}(y_0 - y_0^*) \tag{2.14}$$

for the illustrative construction of the bifurcation diagrams. In the following, we assume for simplicity that the functions τ_C, λ_u, λ_s, a, c, d, x_1^*, y_0^*, and τ_1 are independent of the parameter μ.

The simplest periodic orbits in the system are the fixed points P_n of the mapping $\mathbf{T}_1 \circ \mathbf{T}_0^n$. They are the solutions (x_0, y_0) confined in Σ_0 of the equations

$$x_0 = (\lambda_s)^n [x_1^* - a(y_0 - y_0^*)] \underset{n \to \infty}{\to} 0 \tag{2.15}$$

$$b \cdot \mu = -\tfrac{1}{2} d(y_0 - y_0^*)^2 - c\lambda_s^n [x_1^* - a(y_0 - y_0^*)] + (\lambda_u)^{-n} y_0 \tag{2.16}$$

with the period

$$\tau(P_n) = n\tau_c + \tau_1(x_0, y_0) \tag{2.17}$$

Equations (2.15)–(2.17) generate a sequence of curves parametrized by y_0 in the planes (μ, x_0) and $(\mu, \tau(P_n))$, which constitute our bifurcation diagrams drawn schematically in Fig. 6 in the case d, λ_u, $\lambda_s > 0$. In the other cases, the bifurcation diagrams of the period $\tau(P_n)$ versus the control parameter μ are sketched in Fig. 7.

The fold point of the curves is the locus

$$(\mu)_n' = \frac{y_0^*}{b\lambda_u^n} + O(\lambda_s^n) + O(\lambda_u^{-2n}), \qquad n = 1, 2, 3, \ldots \tag{2.18}$$

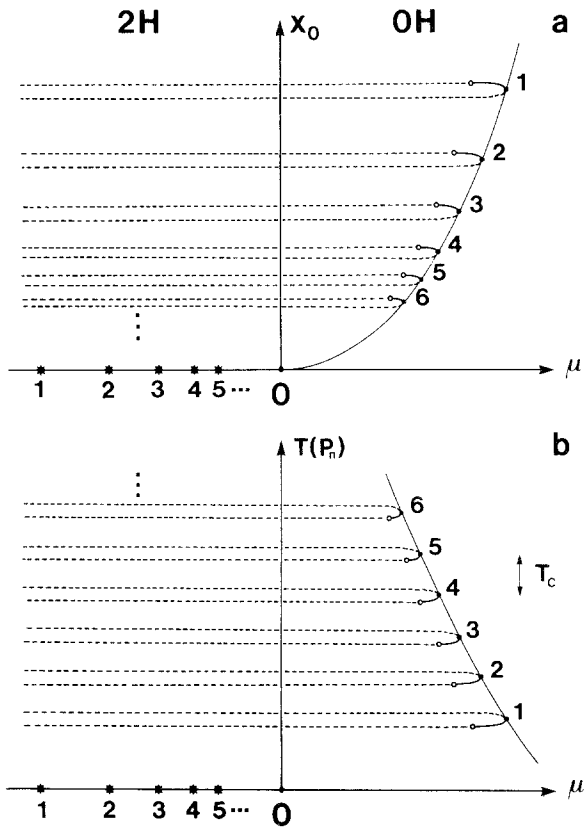

Fig. 6. The schematic bifurcation diagrams of the periodic orbits P_n of (a) the x_0 coordinate and (b) the period $T(P_n)$, versus the parameter μ. The integer associated to each family of periodic orbits is the integer n of P_n. The T_c is the period of the basic periodic orbit C. (●) A tangent bifurcation; (○) a period doubling bifurcation. (—) A stable-node periodic orbit; (- -) a saddle periodic orbit. (∗) A double-circuit homoclinic tangency with its characteristic integer m. The diagrams correspond to the case where all d, $t_{1,v}$, b, y_0^*, x_1^*, a, c, λ_u, and λ_s are positive. The integer followed by H is the number of single-circuit transverse homoclinic orbits on the corresponding side of $\mu = 0$.

where the saddle-node bifurcation occurs. The stable node born at $(\mu)_n^t$ becomes a saddle after a period doubling happening at the parameter value $(\mu)_n^h$, such that

$$(\mu)_n^t - (\mu)_n^h = \frac{2}{bd}\lambda_u^{-2n} + O(\lambda_s^n \lambda_u^{-n}), \qquad n = 1, 2, 3,... \tag{2.19}$$

which is the width of the periodic window of type P_n.

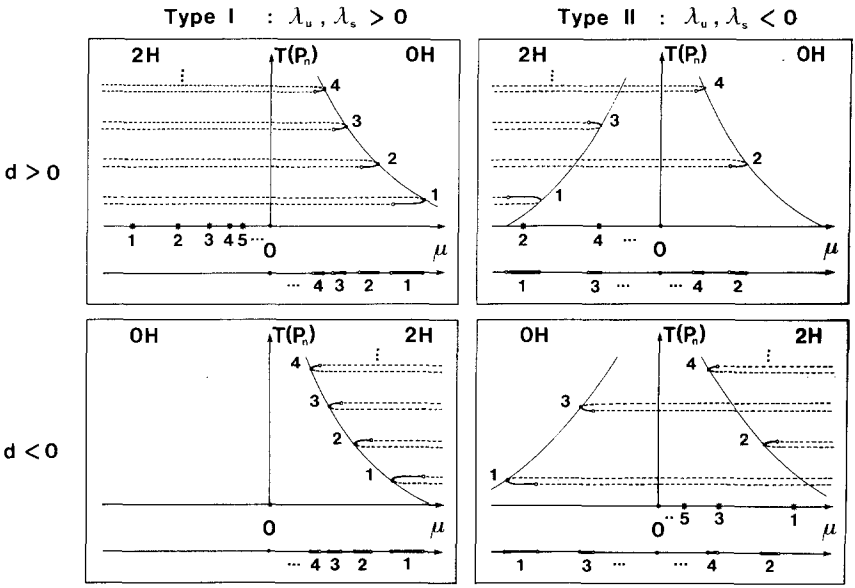

Fig. 7. The schematic bifurcation diagrams of the periodic orbit P_n of the period $T(P_n)$ versus the parameter μ as well as the corresponding diagrams of the periodic windows. t_{1y}, b, y_0^*, x_1^*, a, and c are assumed positive. The same notations as in Fig. 6 are used.

When the map $\mathbf{T}_1$ is regular, as it is the case if its Jacobian (2.13) is not zero, the bifurcation diagram presents a complexity which is well illustrated by the existence of double-circuit homoclinic tangencies similar to those existing in systems with a homoclinic orbit associated to a Shil'nikov saddle focus.[25] They occur at parameter values

$$(\mu)_m^{\varepsilon} = -\frac{c}{b}\lambda_s^m \left[x_1^* - a\varepsilon \left(\frac{2y_0^*}{d\lambda_u^m} \right)^{1/2} + O(\lambda_s^m \lambda_u^{m/2}) \right] \tag{2.20}$$

$$\varepsilon = +, -; \qquad m = 1, 2, 3, \ldots$$

if $y_0^*/d\lambda_u^m$ is positive. Each pair $\pm$ of critical parameter values is represented by a star in Figs. 6 and 7. The existence of these double-circuit homoclinic tangencies triggers an inductive reasoning that shows that the bifurcation diagram is complex and contains a hierarchy of smaller and smaller periodic windows.[25]

However, when the system is strongly contractive, these complex bifurcations and the related chaotic time behaviors may disappear and only the periodic orbits P_n remain in the bifurcation diagram, as we show in the next subsection.

2.2. The Flow Is Strongly Contracting

In chemical kinetics, the flow may be strongly contracting due to the hierarchy of the time scales of the various reaction rates. All the trajectories with different initial conditions are then brought together by the flow.

As a consequence, the map $\mathbf{T}_1$ will have the regular form (2.10)–(2.12) only in an extremely small region in the phase space, because $\mathbf{T}_1$ will map all the trajectories out of the domain Σ_0 into a very small region of Σ_1 which is undistinguishable from a point up to a given precision. For such systems, we should consider the limit case where $\mathbf{T}_1$ is infinitely contractive to a single point of Σ_1 independently of the initial condition and has the following form:

$$\mathbf{T}_1 : \Sigma_0 \to \Sigma_1 \begin{cases} x_1 = x_1^*(\mu) \\ y_1 = b(\mu) \cdot \mu \\ t_1 = t_0 + \tau_1(x_0, y_0, \mu) \end{cases} \tag{2.21}$$

with $(x_0, y_0) \in \Sigma_0$. In this limit case, a continuum of homoclinic orbits forms the homoclinic tangency at $\mu = 0$, whereas no homoclinic orbit exists if $\mu \neq 0$.

Since the whole dynamics is mapped into a single point by $\mathbf{T}_1$, all the possible trajectories of the system coalesce on a single superstable periodic orbit. The only possible trajectories are then the periodic orbits P_n, the basic cycle C, and the main homoclinic orbit P_∞.

Proceeding as before with the form (2.6)–(2.8) of the map $\mathbf{T}_0$, but keeping here the dependence of the parameter μ, one has that the P_n oscillations are fixed points of $\mathbf{T}_1 \circ \mathbf{T}_0^n$ and can be obtained as solutions of the equations

$$x_0 = [\lambda_s(\mu)]^n x_1^*(\mu) \tag{2.22}$$

$$y_0 = [\lambda_u(\mu)]^n b(\mu) \cdot \mu \tag{2.23}$$

$$\tau(P_n) = n\tau_C(\mu) + \tau_1(x_0, y_0; \mu) \tag{2.24}$$

where (x_0, y_0) belongs to $\Sigma_0(\mu)$. The return time function plays a very important role because it determines the shape of the bifurcation diagram in the plane $(\mu, \tau(P_n))$.

The periodic trajectories are here *superstable* with two vanishing Liapunov numbers

$$\Lambda_+(P_n) = \Lambda_-(P_n) = 0 \tag{2.25}$$

Here again the type of the basic periodic orbit C characterizes the ordering of the periodic windows P_n, as shown in Fig. 8. Of course, if the system

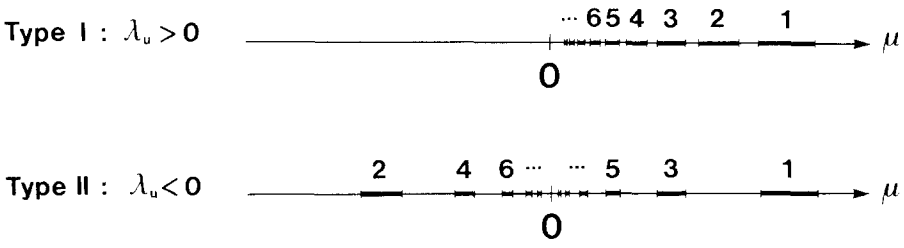

Fig. 8. Ordering of the periodic windows P_n around a homoclinic tangency at $\mu = 0$ when the flow is infinitely contracting. The integer is n of P_n.

(2.1) is analytic, the map $\mathbf{T}_1$ is not infinitely, but only strongly contractive and the set of quasirandom trajectories predicted by Gavrilov and Shil'nikov[22] is then always present, albeit in an extremely small region in the phase space. Such chaotic behaviors will not have a real importance in the natural system if the internal noise level due to thermodynamic or environmental fluctuations is higher than the amplitudes of chaotic variations.

3. THE THERMOKINETIC MODEL

We illustrate the role of homoclinicity in the understanding of the sequence of bifurcations of mixed-mode oscillations by a detailed analysis of a thermokinetic model of hydrocarbon oxidation in the gaseous phase.

3.1. The Model

The combustion in the acetaldehyde–oxygen system in a well-stirred flow reactor has been the object of detailed experiments, which have revealed the existence of various types of periodic time evolutions: cool flame oscillation, ignition oscillation, and several mixed-mode oscillations.[6] The thermokinetic model of hydrocarbon oxidation presented in Ref. 7 reproduces all these time behaviors qualitatively. The reaction scheme adopted in the model is as follows:

1. Initiation:

$$\mathrm{Y} \xrightarrow{\tilde{k}_1} \mathrm{X} \tag{3.1}$$

2. Branching:

$$\mathrm{X} + \mathrm{Y} \xrightarrow{\tilde{k}_2} 2\mathrm{X} + \tilde{h}_2 \tag{3.2}$$

$$\mathrm{X} \xrightarrow{\tilde{k}_3} 2\mathrm{X} + \tilde{h}_3 \tag{3.3}$$

3. Termination:

$$X \xrightarrow{\tilde{k}_4} S_1 + \tilde{h}_4 \tag{3.4}$$

$$X \xrightarrow{\tilde{k}_5} S_2 \tag{3.5}$$

where Y is a molecule of the fuel or the oxygen and X is the chain carrier. Reactions (3.2)–(3.4) are exothermic.

As noted in Ref. 7, complex dynamics as mixed-mode oscillations can only appear if the number of kinetic variables is at least three. They are here the concentrations X and Y and the temperature T, which satisfy the following mass and energy balance equations:

$$\frac{dX}{dt} = k_1(u)\, Y + k_2(u)\, XY + [k_3(u) - k_4(u) - k_5 - 1]\, X \tag{3.6}$$

$$\frac{dY}{dt} = -[k_1(u) + 1]\, Y - k_2(u)\, XY + 1 \tag{3.7}$$

$$\frac{du}{dt} = [h_2 k_2(u)\, Y + h_3 k_3(u) + h_4 k_4(u)]\, X - k_T u \tag{3.8}$$

where $u = (T - T_0)/T_0$ is the relative temperature with respect to the ambient temperature T_0. The reaction rates k_1 to k_4 depend on the relative temperature as shown in Table I. The unit of the concentrations X and Y chosen is scaled to the inflow concentration of fuel and oxygen, assumed to be equal. The unit of time t is the residence time in the reactor. The term $k_T u$ represents a Newtonian heat loss.[32] The reactant pressure P is chosen near 553 mm Hg and the ambient temperature T_0 is the bifurcation parameter.

Table I. Reaction Rates and Various Constants for the Thermokinetic Reaction (3.1)–(3.5)[a]

$k_1 = 4A_1 N_0 e^{-e_1/(1+u)}$	$A_1 = 1.6 \times 10^{10}$	$E_1 = 24$	$\tilde{h}_1 = 0$
$k_2 = 2A_2 N_0 e^{-e_2/(1+u)}$	$A_2 = 7.4 \times 10^{12}$	$E_2 = 25$	$\tilde{h}_2 = 92$
$k_3 = 4A_3 N_0 e^{-e_3/(1+u)}$	$A_3 = 1.38 \times 10^{8}$	$E_3 = 7$	$\tilde{h}_3 = 4$
$k_4 = 4A_4 N_0 e^{-e_4/(1+u)}$	$A_4 = 7.8 \times 10^{10}$	$E_4 = 16$	$\tilde{h}_4 = 20$
$k_5 = A_5 N_0^{1/2}$	$A_5 = 3.3 \times 10^{3}$	$E_5 = 0$	$\tilde{h}_5 = 0$
$k_T = (4 \times 3.68 \times 10^{-4}/11)$ (cm^{-3} mole) $\times N_0^{-1}$			
$N_0 = P/RT_0$ with $P/R = 560/(760 \times 83.144)$ (cm^{-3} mole K)			
$e_j = E_j/RT_0$, $j = 1, 2, 3, 4$, with $R = 1.987$ (cal mole^{-1} K^{-1})			
$h_j = \tilde{h}_j/[22$ (cal mole^{-1} K^{-1}) $\times T_0]$			

[a] Units of A_1–A_4 are cm^3 mole^{-1}; of A_5, cm$^{3/2}$ mole$^{-1/2}$; of E's and $\tilde{h}$'s, kcal mole^{-1}.

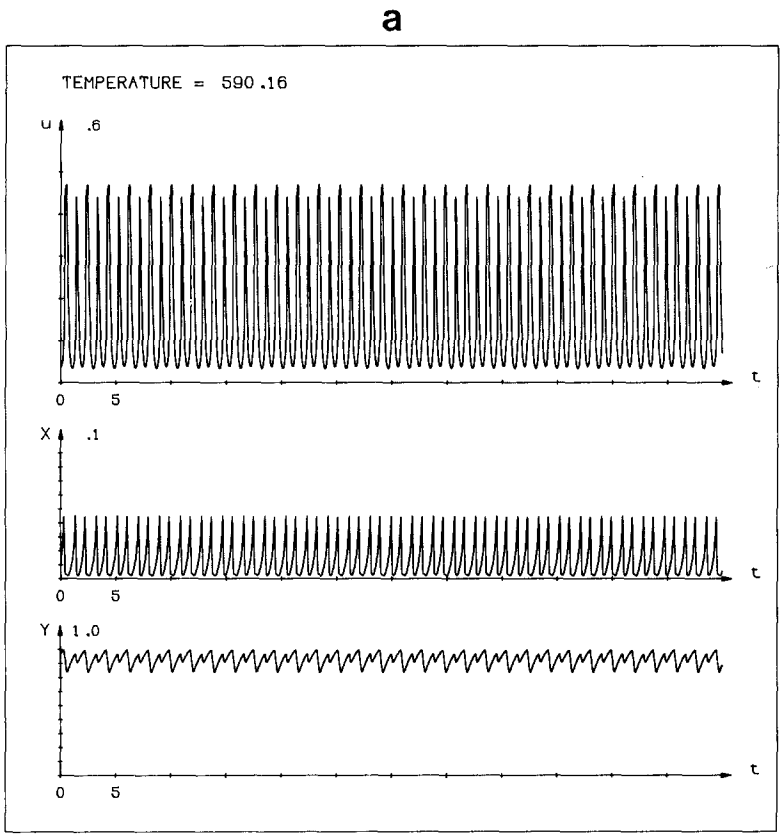

Fig. 9. (a) Doubled cool flame oscillation at $T_0 = 590.16$; (b) Chaotic cool flame oscillation at $T_0 = 590.13$.

As the ambient temperature T_0 is decreased, five regions of different dynamical behaviors are observed[7]:

Region V. A stable focus steady state at moderately high temperature undergoes a Hopf bifurcation at

$$(T_0)_{\text{IV-V}} = 623 \text{ K} \tag{3.9}$$

and gives birth to the following behavior:

Region IV. Cool flame oscillations arise, which are periodic and smooth. The temperature variation in cool flames remains bounded below 400 K. The cool flame limit cycle becomes unstable by a period doubling at

$$(T_0)_c^h = 590.24273 \text{ K} \tag{3.10}$$

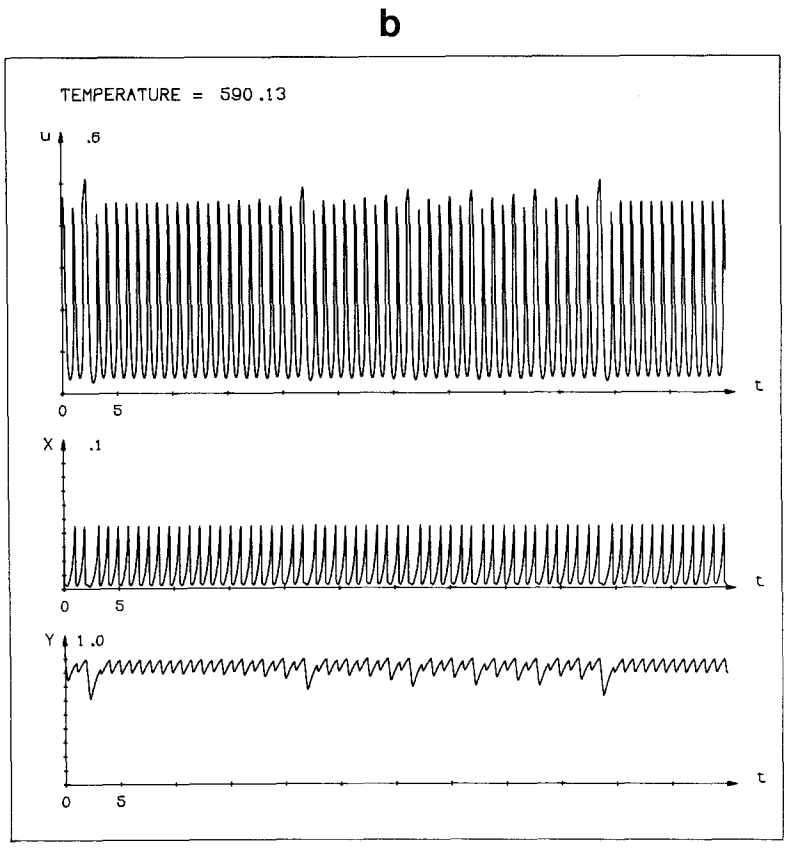

Fig. 9 (*continued*)

An example of doubly periodic cool flame oscillations is shown in Fig. 9a. Let us remark that the variation in the peak amplitude in the doubling is small. As the ambient temperature T_0 still decreases, cool flame oscillations undergo a period doubling cascade,[30] leading to *chaotic cool flame oscillations*. An example is shown in Fig. 9b. Next, the amplitude of the cool flame oscillations reaches a critical threshold where ignition starts, as explained in Section 5.

Region III. So, below the critical temperature

$$(T_0)_{\text{III-IV}} = 590.1295 \text{ K} \tag{3.11}$$

mixed-mode periodic oscillations occur. They are composed of several cool flame peaks of temperature variation of about 400 K separated by an

ignition peak where the temperature rises up to several thousand kelvin degrees. Figure 13 displays an example. The number of cool flame peaks changes in an apparently irregular sequence of bifurcations as the ambient temperature T_0 decreases. Only periodic mixed-mode oscillations were observed numerically in the model with certainty. They are presented in Table III.

According to the analysis to be presented below, we can understand the mechanism at the origin of this complex bifurcation sequence as follows. When the chaotic cool flame oscillations are generated by bifurcations in region IV, a Smale horseshoe of cool flame oscillations is created. In region III, this Smale horseshoe is a hyperbolic repellor. The high fuel consumption during ignition causes the reinjection in the vicinity of the hyperbolic repellor of cool flames. So a homoclinic tangency to the Cantor set of cool flame trajectories exists, which explains globally the sequence of bifurcations, as we show in Section 5.

Section 4 is concerned with the low-ambient-temperature part of the sequence, where at T_{0H}, there is an example of homoclinic tangency to a periodic orbit. This latter is the unstable cool flame orbit of lowest period, which was stable in region IV for $T_0 > (T_0)_c^h$. A regular sequence of mixed-mode oscillations is organized around the homoclinic tangency. The sequence of mixed-mode oscillations ends at

$$(T_0)_{\text{II-III}} = 585.8 \text{ K} \tag{3.12}$$

Region II. Below this temperature there exist relaxation oscillations of simple ignition, which disappear at

$$(T_0)_{\text{I-II}} = 563 \text{ K} \tag{3.13}$$

Region I. The attractor is then a stable node steady state at low temperature.

3.2. Numerical Computation of the Periodic Orbits

The periodic orbits, their stability, and their bifurcation loci in the parameter space are computed by Newton's method of the tangent developed by Sparrow.[26]

Sinai and Vul[27] and De Gregorio[28] argued how a rigorous proof of existence of a periodic orbit can be provided by such a method.

Let us denote by

$$\mathbf{X}_1 = \boldsymbol{\phi}(t_0; \mathbf{X}_0, \mu) \tag{3.14}$$

the mapping generated by the flow (2.1) from the initial condition $\mathbf{X}_0$ during a time t_0. The system (2.1) admits a trajectory of period τ^* through a point $\mathbf{X}^*$ in the section plane $\mathbf{a} \cdot \mathbf{X} = b$ if these values are solutions of

$$\mathbf{X}^* = \boldsymbol{\phi}(\tau^*; \mathbf{X}^*, \mu) \qquad \text{with} \quad \mathbf{a} \cdot \mathbf{X}^* = b \tag{3.15}$$

If approximations $\mathbf{X}_0$ and τ_0 to these values are known, they differ from the true values by corrections

$$\mathbf{X}^* = \mathbf{X}_0 + d\mathbf{X}_0, \qquad \tau^* = \tau_0 + d\tau \tag{3.16}$$

Introducing (3.16) into Eq. (3.15), dropping the terms nonlinear in the corrections, and using (3.14) and the fact that

$$\frac{\partial \boldsymbol{\phi}}{\partial t}(\tau_0; \mathbf{X}_0, \mu) = \mathbf{F}_\mu(\mathbf{X}_1)$$

we obtain the equations satisfied by the corrections:

$$\begin{aligned} \left[I - \frac{\partial \boldsymbol{\phi}}{\partial \mathbf{X}}(\tau_0; \mathbf{X}_0, \mu) \right] d\mathbf{X} - \mathbf{F}_\mu(\mathbf{X}_1)\, d\tau &= \mathbf{X}_1 - \mathbf{X}_0 \\ \mathbf{a} \cdot d\mathbf{X} &= 0 \end{aligned} \tag{3.17}$$

which form an inhomogeneous linear system of four equations with four unknown quantities. Given the approximate elements $\mathbf{X}_0$, τ_0 of the periodic orbit, we need to integrate the differential equation system (2.1) with the linearized system

$$\dot{\mathbf{X}}(t) = \mathbf{F}_\mu(\mathbf{X}(t))$$

$$\dot{\mathscr{L}}(t) = \frac{\partial \mathbf{F}_\mu}{\partial \mathbf{X}}(\mathbf{X}(t)) \cdot \mathscr{L}(t)$$

to provide

$$\mathbf{X}_1 = \boldsymbol{\phi}(\tau_0; \mathbf{X}_0, \mu) \qquad \text{and} \qquad \mathscr{L}(\tau_0) = \frac{\partial \boldsymbol{\phi}}{\partial \mathbf{X}}(\tau_0; \mathbf{X}_0, \mu)$$

These expressions are then inserted into the system (3.17) to compute more precisely elements of the periodic orbit by Eqs. (3.16). The iteration is carried on three or four times to obtain a sufficiently good approximation of $\mathbf{X}^*$, τ^*. The advantage of the Newton method is its superconvergence. Independently of the stability of the periodic orbit, provided that the latter is not marginal, the initial error ε is reduced to ε^{2^n} after n iterations. This stability is given by the eigenvalues of the integrated linearized system

$$\mathscr{L}(\tau^*) = \frac{\partial \boldsymbol{\phi}}{\partial \mathbf{X}}(\tau^*; \mathbf{X}^*, \mu)$$

The periodic orbit of a nearby parameter value is computed by extrapolation with a linear increment in the parameter $\mu \to \mu + d\mu$. The linear variations dX, $d\tau$, and $d\mu$ then satisfy a linear system similar to (3.17), which depends, furthermore, on $(\partial \boldsymbol{\phi}/\partial \mu)(\tau^*; \mathbf{X}^*, \mu)$. This system is solved to obtain the variations $(d\mathbf{X}, d\tau, d\mu)$ either for a given parameter increment $d\mu$ if $d\tau/d\mu < 1$, or for a given increment of the period $d\tau$ if $d\tau/d\mu > 1$.

The integration of the 15 variables $(\boldsymbol{\phi}, \partial \boldsymbol{\phi}/\partial \mathbf{X}, \partial \boldsymbol{\phi}/\partial \mu)$ was performed by a variable-order, variable-step Gear method of the NAG library[29] to handle the stiffness of the differential equation system.

4. HOMOCLINIC TANGENCY TO THE BASIC CYCLE

The aforementioned method was used to follow the mixed-mode periodic orbits P_n as well as the basic periodic orbit C to which is associated the tangent homoclinic orbit in the model (3.6)–(3.8).

The sequence of the mixed-mode oscillations below $T_0 \simeq 589.9966$ is drawn in Fig. 10 in comparison with the basic cycle. The bifurcation diagram of their period versus the ambient temperature T_0 is presented in Fig. 11 up to the oscillation P_7. The bifurcation diagram of the oscillations from P_3 to P_{10} is shown in a logarithmic scale in Fig. 12, which proves the exponential accumulation at the critical temperature T_{0H}. This critical temperature was determined by its localization in the interval between two temperatures T_0 of occurrence of the oscillations P_{19} and P_{20} and is given by

$$T_{0H} = 589.459801925 \pm 15 \times 10^{-9} \tag{4.1}$$

where the homoclinic tangency to the basic cycle C occurs.

The oscillations with n even occur for $T_0 > T_{0H}$, those with n odd for $T_0 < T_{0H}$. The origin of this feature is in the negative sign of the Liapunov number λ_u of the basic cycle C. In fact, one finds

$$|\lambda_s(\mu)| \leqslant 10^{-8} \tag{4.2}$$

$$\lambda_u(\mu) = -2.56599523 + 3.15876\mu - 2.0961\mu^2 \tag{4.3}$$

$$\tau_C(\mu) = 0.9641756315 - 0.06426701\mu + 0.0080859\mu^2 \tag{4.4}$$

where $\mu = T_0 - T_{0H}$ varies between -0.06 and 0.04.

The Liapunov number $\lambda_u(0)$ and the period $\tau_C(0)$ govern the scaling properties of the bifurcation diagram of Figs. 11 and 12, as shown in

Table II. In this table $(\mu)_n^1$ [resp. $(\mu)_n^2$] denotes the boundary of the periodic window P_n that is the closest to (resp. the farthest from) the homoclinic tangency $\mu = 0$ and $\tau^I(P_n)$ is the period of the oscillation P_n at $(\mu)_n^I = 2.3[\lambda_u(0)]^{-n}$.

The oscillations P_1 and P_2 differ from the oscillations $P_3, P_4, \ldots$. Indeed, P_1 undergoes a tangent bifurcation localized by the arrow in

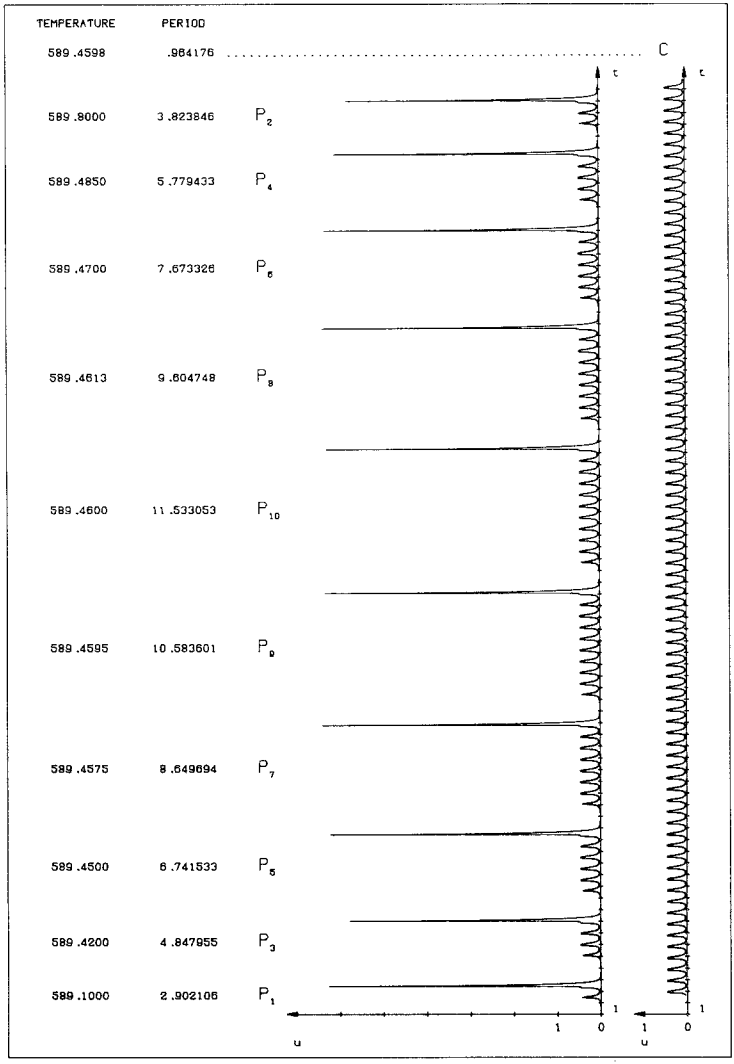

Fig. 10. The sequence of mixed-mode oscillations of the thermokinetic model (3.6)–(3.8). The variations in the relative temperature $u = (T - T_0)/T_0$ are represented. Displayed below is the unstable basic periodic orbit C at the homoclinic tangency T_{0H}.

Fig. 11. However, no such tangent bifurcation occurs for all the other oscillations P_n, which remain superstable within the precision of the integration. Furthermore, the maximum temperature of the ignition peak of P_2 decreases as the boundary $(\mu)_n^2$ is approached, although it remains roughly constant for $P_3, P_4, \ldots$.

The approach of the boundary $(\mu)_n^2$ is characterized by a thickening of the cool flame temperature oscillation two peaks before the ignition peak and with the deepening of the oscillation in the fuel concentration Y, as shown in Fig. 13b for P_5. All the mixed-mode oscillations P_n from P_3 with n increasing are accounted for by a homoclinic tangency occurring at T_{0H} and associated with the basic cool flame oscillation C.

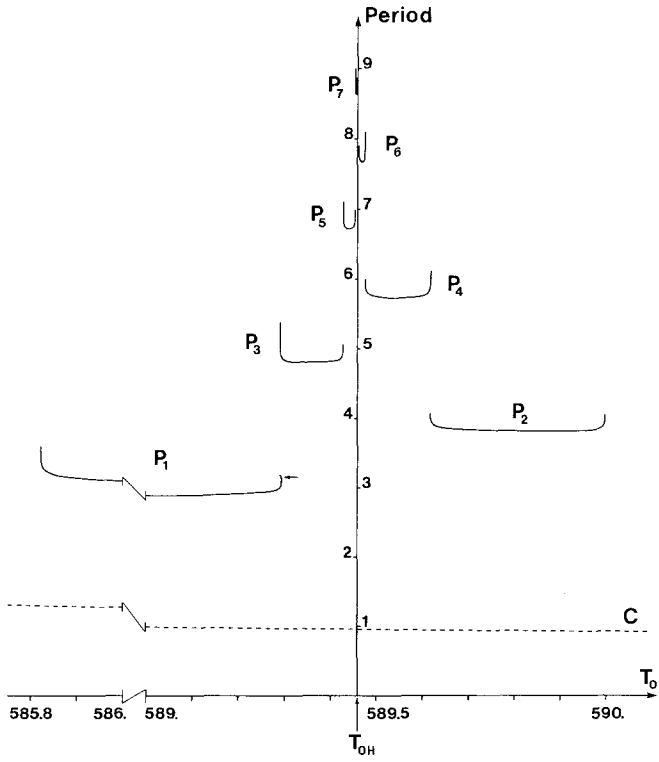

Fig. 11. Bifurcation diagram of the mixed-mode oscillations P_n of the period versus the ambient temperature T_0. Here T_{0H} is the temperature of the homoclinic tangency. The curve C is the period of the basic cycle C. The arrow on the curve of P_1 denotes the locus of a tangent bifurcation. The curve P_1 above the arrow corresponds to a saddle periodic orbit P_1. All the other periodic orbits P_n are stable with two Liapunov numbers vanishing within the precision of the computation. The basic cycle C is a saddle.

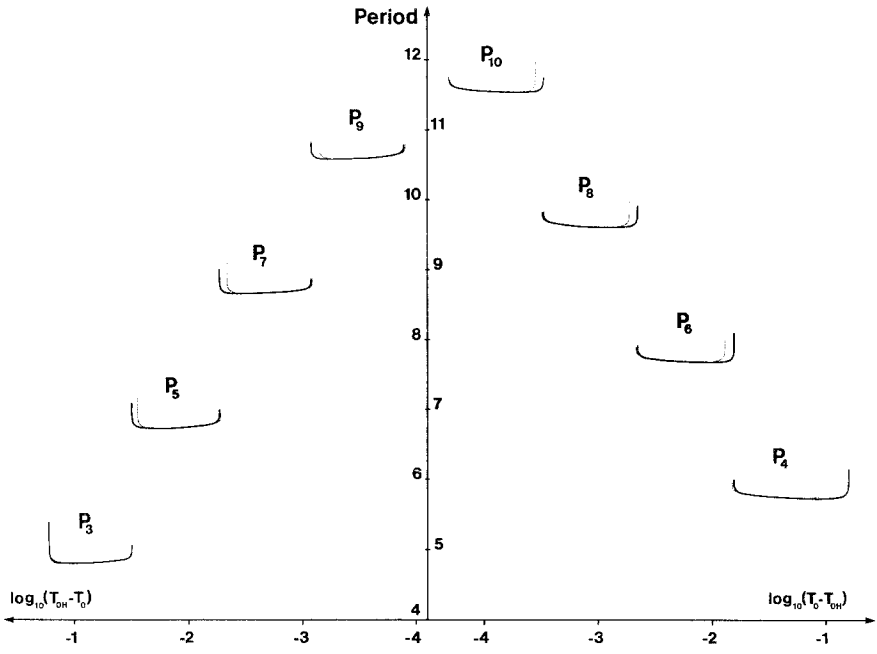

Fig. 12. Bifurcation diagram of the mixed-mode oscillations from P_3 to P_{10} of the period versus the decimal logarithm of the difference $|T_0 - T_{0H}|$, with T_{0H} given by (4.1). The bifurcation diagram computed from the Poincaré mapping is superposed in dots.

The homoclinicity is revealed by the numerical construction of a Poincaré mapping. The section plane chosen is

$$X = 0.022 \tag{4.5}$$

transverse to the cycle C.

The local stable and unstable manifolds of the cycle C were computed. Several trajectories of the unstable manifold were then integrated up to the return in the section plane after a given time. Figure 14 depicts the time variation along a tangent homoclinic orbit occurring when the return belongs to the local stable manifold. The computation shows that all the different initial conditions near the cycle C are mapped on a single point within the precision 10^{-7} in the phase space, whereas the return time depends sharply on the initial condition on the local unstable manifold. The map $\mathbf{T}_1$ is thus strongly contractive of the form (2.21). The map $\mathbf{T}_1$ is defined as the mapping from the section plane (4.5) with a return on itself at a time longer than 3.5. The coordinates x and y of a point in the section

Table II. Accumulation Rates, at the Homoclinic Tangency, of the Boundaries $(\mu)_n^1$, $(\mu)_n^2$ of the Periodic Windows P_n and of the Periods $\tau^1(P_n)$ of the Oscillation P_n at $(\mu)_n^1 = 2.3[\lambda_u(0)]^{-n}$

n	$(\mu)_n^1$	$(\mu)_n^2$	$[(\mu)_{n-2}^1/(\mu)_n^1]^{1/2}$	$[(\mu)_n^2/(\mu)_{n+2}^2]^{1/2}$	$\tau^1(P_n)$	$[\tau^1(P_n)-\tau^1(P_{n-2})]/2$
1	−0.1678461	−3.6386926	—	4.6561	2.89787	—
3	−0.0316355	−0.16784	2.303396	2.304	4.81301	0.95757
5	−0.0053490	−0.031626	2.43192	2.432	6.72109	0.95404
7	−0.000837	−0.005349	2.528	2.529	8.64283	0.96087
9	−0.000128	−0.000836	2.56	—	10.56993	0.96355
2	0.1584894	0.536780	—	1.840992	3.82293	—
4	0.0156035	0.158377	3.18706	3.186	5.74152	0.95929
6	0.0022046	0.01560	2.66037	2.661	7.67518	0.96683
8	0.000330	0.002204	2.585	2.587	9.60518	0.96500
10	0.0000501	0.000329	2.566	—	11.53415	0.96448
			$\lambda_u(0) = -2.56599523$			$\tau_c(0) = 0.9641756315$

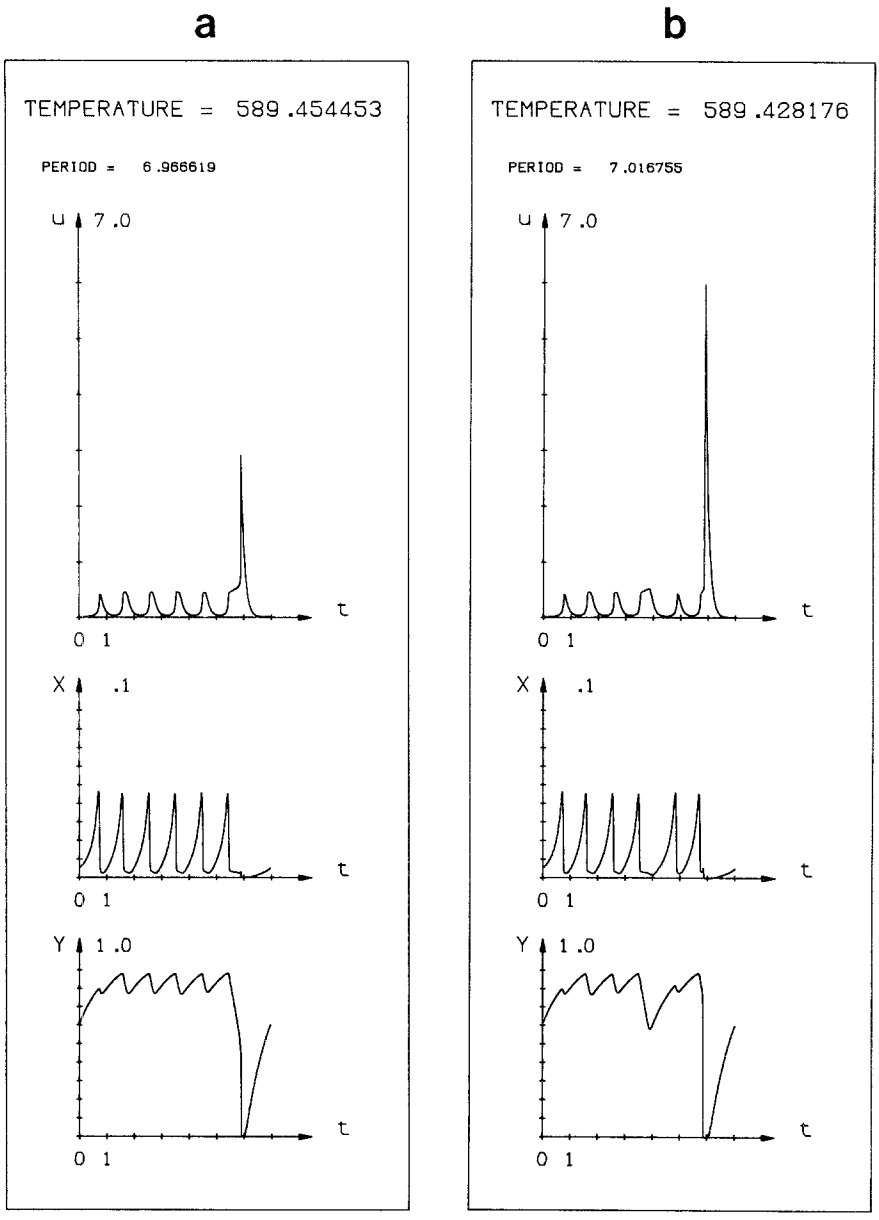

Fig. 13. The mixed-mode oscillation P_5 near the boundaries (a) $(\mu)_n^1$ and (b) $(\mu)_n^2$ compared with (c) the unstable basic cycle C, in the temperature u and the two concentrations X and Y. The oscillation shape in part (a) is the most typical of the periodic window.

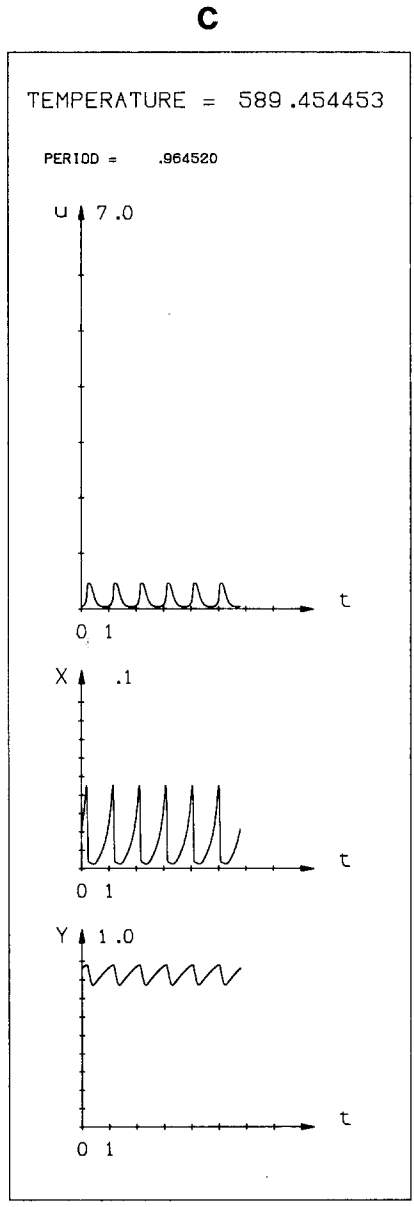

Fig. 13 (*continued*)

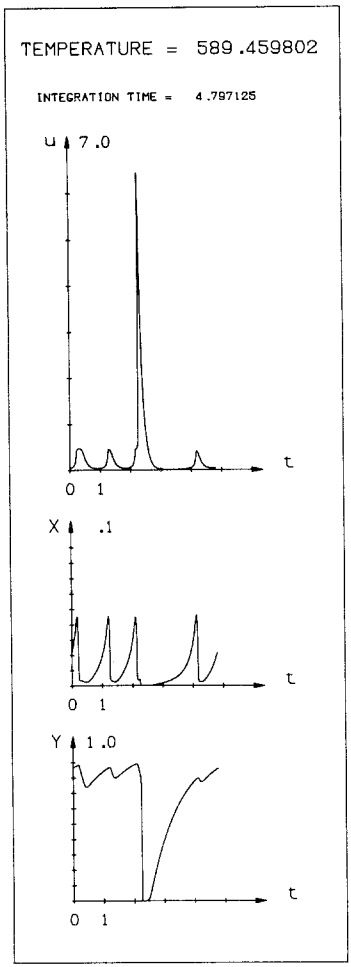

Fig. 14. The homoclinic orbit of the homoclinic tangency at $\mu = 0$, integrated from initial condition $x_0^* = 0$, $y_0^* = 0.003$ up to $x_1^* = 0.00000234$, $y_1^* < 10^{-8}$ in the local coordinates (x, y) of the section plane $X = 0.022$. The whole homoclinic orbit converges to the basic cycle C in the past and the future. (Note that, since the flow is strongly contractive, all the various initial conditions are mapped onto a region of order 10^{-7} on the section plane. So the initial condition of the orbit of the unstable manifold where the tangency to the stable manifold occurs is undetermined within this precision. Unicity in the determination of the homoclinic orbit is not guaranteed, because the unstable manifold may be rolled on itself by the flow in a region smaller than 10^{-7}.)

plane (4.5) denote its projections on directions tangent to the stable and unstable manifolds, respectively, of the basic cycle C. The stable and unstable directions are represented by unit vectors in the section plane (4.5).

The different functions of the map $\mathbf{T}_1$ in (2.21) are then given by

$$x_1^*(\mu) = 0.000002336 + 0.00000456\mu + 0.0003097\mu^2 \tag{4.6}$$

$$b(\mu) = -0.0185328 + 0.000688\mu \tag{4.7}$$

The computed return time function is shown in Fig. 15 and is fitted by

$$\tau_1(y_0, \mu) = \frac{p(\mu) + q(\mu)\, y_0}{[y_0 - s_1(\mu)]^{\alpha_1}\, [s_2(\mu) - y_0]^{\alpha_2}} \tag{4.8}$$

with $\alpha_1 = 1/215, \qquad \alpha_2 = 1/106$

$$p(\mu) = 4.424 - 0.05\mu \tag{4.9}$$

$$q(\mu) = -21.7 + 42\mu - 130\mu^2 \tag{4.10}$$

$$s_1(\mu) = 0.00065963 + 0.0024348\mu + 0.004171\mu^2 \tag{4.11}$$

$$s_2(\mu) = 0.00380534 + 0.0043385\mu + 0.001891\mu^2 \tag{4.12}$$

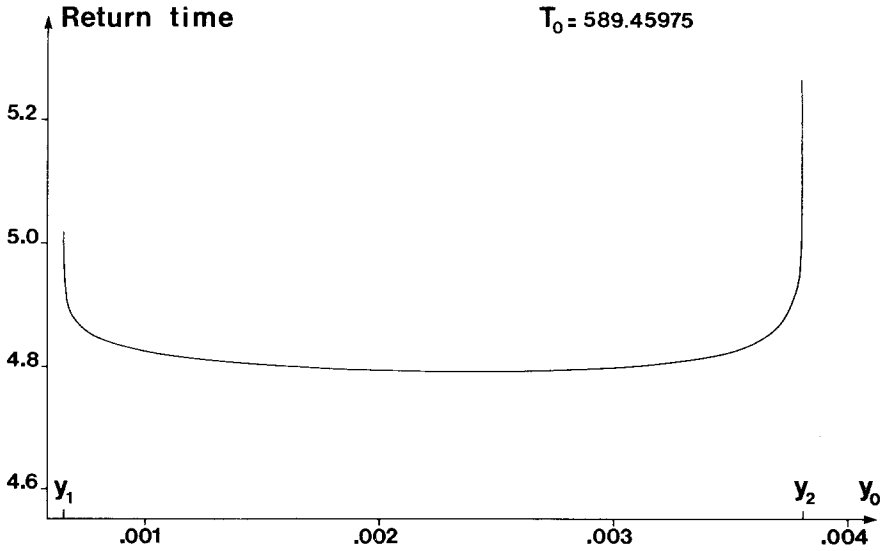

Fig. 15. The return time versus the initial condition y_0 on the local unstable manifold, at $T_0 = 589.45975$, in the case corresponding to the homoclinic orbit of Fig. 14. For different parameter values the function is similar, but with shifted boundaries s_1 and s_2.

defined on

$$-0.06 \leqslant \mu \leqslant 0.04$$

$$y_1(\mu) = s_1(\mu) + 2 \times 10^{-7} \leqslant y_0 \leqslant s_2(\mu) - 4 \times 10^{-8} = y_2(\mu) \qquad (4.13)$$

Its dependence on x_0 is negligible.

This specific form with two divergences at $s_1(\mu)$ and $s_2(\mu)$ was chosen empirically because the numerical return time seems to diverge at the boundaries of its domain of definition. We do not know the mechanism of the origin of these apparent divergences, so we do not know whether they are exact or not. However, we have observed no saturation behavior. The exponents α_1 and α_2 were chosen within an uncertainty interval of 10% by fitting a straight line in the log–log plot of the return time function versus $|y_0 - y_i(\mu)|$, $i = 1, 2$. Up to a certain degree the choice of the form of $\tau_1(y_0, \mu)$ and of α_1 and α_2 is arbitrary, but we present precise fitted parameters and functions without errors because we intend to use them as a definite submodel.

The characteristic shape of the return time function appears in the bifurcation diagram in Fig. 12, because the period of the periodic orbit P_n depends on it by Eq. (2.24) As μ tends to $(\mu)_n^1$ [resp. $(\mu)_n^2$], y_0 of Eq. (2.23) approaches $y_1(\mu)$ [resp. $y_2(\mu)$]. In Fig. 12 the superposed dots give the bifurcation diagram of the fixed points of the maps $\mathbf{T}_0^{n-3} \circ \mathbf{T}_1$ with $n = 3, 4, 5, \ldots, 10$ corresponding to the periodic orbits P_n.[4]

Near the boundaries $(\mu)_n^1$, the agreement is very good. The discrepancy occurring near the boundaries $(\mu)_n^2$ is due to the aforementioned thickening of one of the cool flame peaks (see Fig. 13b). This behavior forces the periodic orbit to leave the domain where the map $\mathbf{T}_0$ has the simple linear form (2.6)–(2.9). A nonlinear form should take account of this feature, as shown in Section 5. The discrepancy is not present on the period of P_3 because it is a fixed point of $\mathbf{T}_1$ alone.

In Fig. 12, the periodic windows are juxtaposed, leaving no visible room to any further dynamical behaviors. Nevertheless, we found a gap between the windows P_3 and P_5 (see Table II) filled by a very small periodic window P_7', which differs from P_7 by the existence of a thick, fourth cool flame peak in the period. This feature of the shape means that the oscillation P_7' does not belong to the fixed points of $\mathbf{T}_1 \circ \mathbf{T}_0^k$. Indeed, there exists another homoclinic orbit, which is displayed in Fig. 16, with another map $\mathbf{T}_1'$ with a longer return time, but which is defined only on a very small domain

$$0.00380534 < y_0 < 0.00380555 \qquad (4.14)$$

[4] The use of $n = 3$ supposes that $x_1^*(\mu) \simeq 0$, which is satisfied here [see (4.6)].

The smallness of this domain with respect to (4.13) explains why a family of periodic orbits derivating from $\mathbf{T}_1'$ has not been observed numerically. However, this fact shows that the classification of the mixed-mode oscillations into a sequence P_n is too poor to describe the trajectories of the thermokinetic system, because it does not distinguish thick from thin cool flame oscillations, so that we should enlarge the classification scheme.

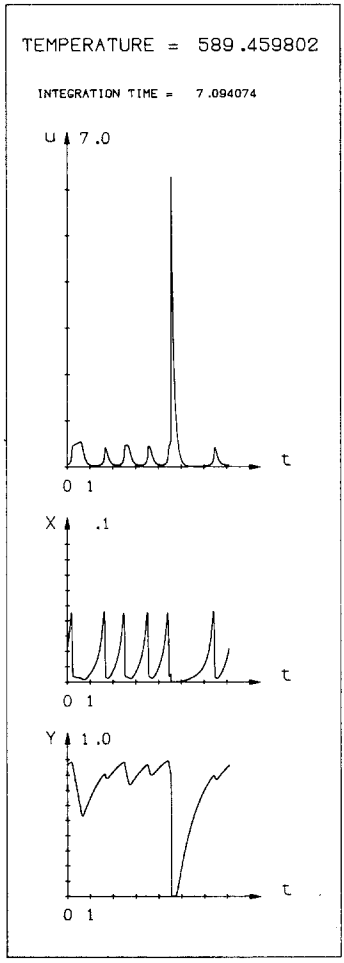

Fig. 16. The homoclinic orbit $10^3 I 0^\infty$ of the homoclinic tangency of the second kind occurring at $\mu = 0$, computed from initial condition $x_0^* = 0$, $y_0^* = 0.00380543$ up to $x_1^* = 0.00000234$, $y_1^* < 10^{-8}$ in the local coordinates (x, y) of the section plane $X = 0.022$. This homoclinic tangency is at the origin of the oscillation P_7' observed between P_3 and P_5.

5. HOMOCLINIC TANGENCY TO A CANTOR SET OF TRAJECTORIES

Our goal in this section is to understand the complete bifurcation sequence in region III of oscillations of mixed cool flame and ignition oscillations, which is presented in Table III.

5.1. Cool Flame and Ignition Subdynamics

As for the sequence of mixed-mode oscillations analyzed in Section 4, two mappings are required, describing, respectively, the cool flame subdynamics, denoted here by $\mathbf{T}_{CF}$ (CF for cool flame), and the ignition subdynamics, denoted here by $\mathbf{T}_I$ (I for ignition). They are replacing $\mathbf{T}_0$ and $\mathbf{T}_1$, respectively.

As presented in Section 3.1, we know that a (nonattracting) Smale horseshoe exists in the cool flame subdynamics in region III. This Smale horseshoe constitutes a hyperbolic repellor. Its existence is proved here, but we shall not study its creation. The presence of this horseshoe is related to the observation in the preceding section that there exist two types of cool flame peaks: thin and thick peaks as they appear in the temperature signal. Compare Figs. 9 and 13. These features suggest that the map $\mathbf{T}_{CF}$ describing the cool flame subdynamics is indeed nonlinear of logistic type rather than linear as was $\mathbf{T}_0$.

The maps $\mathbf{T}_{CF}$ with $\mathbf{T}_I$ were constructed numerically for three values of the ambient temperature T_0. They are plotted in Figs. 17a, 18a, and 18b. The section plane is the same as in Section 4 [see Eqs. (4.5)] and y is the coordinate on a unit vector in the section plane tangent to the unstable manifold of the basic cycle C. Due to the strong contractivity of the thermochemical dynamics, the map $\mathbf{T}_{CF}$ appears to be quasi-one-dimensional and the map $\mathbf{T}_I$ pointlike, because ignition is even more contractive.

As mentioned earlier, the map $\mathbf{T}_{CF}$ below the value y^* is of logistic type. But the cool flame system is a hyperbolic repellor because the top of the function is outside the definition interval of the 1D map $\mathbf{T}_{CF}$ bounded by the threshold y^*. The trajectories will then leave this definition interval through an interval contained in the interval (b', b). The system then undergoes an ignition peak and the trajectories are reinjected in the definition domain of $\mathbf{T}_{CF}$ by the map $\mathbf{T}_I$ at the right in Figs. 17a, 18a, and 18b. Let us represent the map $\mathbf{T}_{CF}$, which is two-dimensional before any approximation, by the equations

$$\mathbf{T}_{CF} \begin{cases} y' = F_{CF}(y, x; T_0) \\ x' = G_{CF}(y, x; T_0) \\ t' = t + \tau_{CF}(y, x; T_0) \end{cases} \qquad (x, y) \in \Delta_0 \cup \Delta_1 \qquad (5.1)$$

where $\Delta_0 \cup \Delta_1$ is the definition domain of $\mathbf{T}_{CF}$.

Table III. Numerical Values of the Observed Mixed-Mode Oscillations in Region III at a Pressure near 553 mm Hg[a]

Ambient temperature T_0		N	Type
564	−585.8	0 (region II)	(I)
585.8211093	−589.2919558	1	$(0I) = P_1$
589.2919577	−589.4281664	3	$(010I) - (0^3I) = P_3$
589.4281674	−589.4281675	7	$(0^310^3I) = P'_7$
589.4281678	−589.4544529	5	$(0^310I) - (0^5I) = P_5$
589.4544534	−589.4589649	7	$(0^510I) - (0^7I) = P_7$
589.4589657	−589.4596739	9	$(0^710I) - (0^9I) = P_9$
589.45968	−589.45978	11	$(0^910I) - (0^{11}I) = P_{11}$
589.459785	−589.459795	13	$(0^{11}10I) - (0^{13}I) = P_{13}$
589.4598	−589.459801	15	$(0^{13}10I) - (0^{15}I) = P_{15}$
589.4598017	−589.4598018	17	$(0^{15}10I) - (0^{17}I) = P_{17}$
589.45980186	−589.45980191	19	$(0^{17}10I) - (0^{19}I) = P_{19}$
589.45980194		20	$(0^{20}I) = P_{20}$
589.459802		18	$(0^{18}I) = P_{18}$
589.4598022	− 589.459803	16	$(0^{16}I) - (0^{14}10I) = P_{16}$
589.459807		14	$(0^{14}I) = P_{14}$
589.45981		12	$(0^{12}I) = P_{12}$
589.4598520	−589.4601312	10	$(0^{10}I) - (0^810I) = P_{10}$
589.4601319	−589.4620057	8	$(0^8I) - (0^610I) = P_8$
589.4620066	−589.4754037	6	$(0^6I) - (0^410I) = P_6$
589.4754054	−589.618178	4	$(0^4I) - (0^210I) = P_4$
589.6182911	−589.9965818	2	$(0^2I) = P_2$
589.99685		22	$(I0^210^{19})$
589.997		12	$(I0^210^9)$
589.99749		10	$(I0^210^510)$
589.9975		12	$(I0^210^510^3)$
589.9975025	−589.997504	14	$(I0^210^510^5)$
589.9975045	−589.9975048	16	$(I0^210^510^7)$
589.9975049		20	$(I0^210^510^710^3)$
589.997505		18	$(I0^210^510^9)$
589.99750515		20	$(I0^210^510^{11})$
589.99750525		22	$(I0^210^510^{13})$
589.99750528		24	$(I0^210^510^{15})$
589.9975053	−589.99750531	26	$(I0^210^510^{17})$
589.99750533		37	$(I0^210^510^{28})$
589.99750534		29	$(I0^210^510^{20})$
589.99750535		27	$(I0^210^510^{18})$
589.997505355	−589.997505365	25	$(I0^210^510^{16})$
589.99750537	−589.99750539	23	$(I0^210^510^{14})$
589.9975054		21	$(I0^210^510^{12})$
589.99750545	−589.9975055	19	$(I0^210^510^{10})$
589.997508	−589.9977	8	$(I0^210^5)$
589.999	−590	6	$(I0^210^3)$
590.01	−590.1226	4	$(I0^210) - (I0^4)$
590.1227		21	$(I0^410^{10}10^5)$
590.123		46	$(I0^410^{29}10^9)$
590.125		12	$(I0^410^7)$
590.126		14	$(I0^410^510^3)$
590.14		∞ (region IV)	(0)

[a] N denotes the number of cool flame peaks in the period. The type is represented by the symbols of the alphabet $\{0, 1, I\}$.

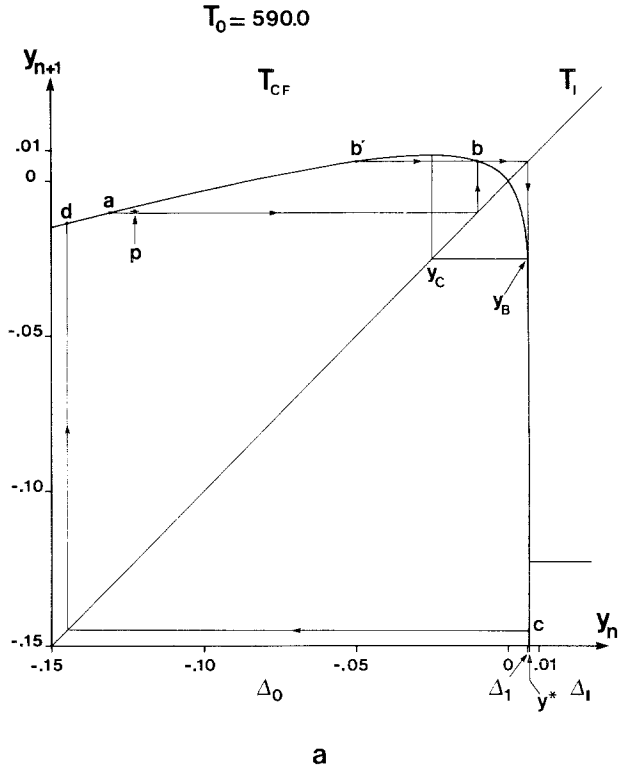

Fig. 17. (a) Return mapping in the section plane $X = 0.022$ at the ambient temperature $T_0 = 590.0$. Here y is the coordinate of the projection of the intersection point onto the axis tangent to the unstable manifold of the basic cycle. The mapping is composed of two maps $\mathbf{T}_{CF}$ and $\mathbf{T}_I$. Point p is the image by $\mathbf{T}_{CF}$ of the reinjection point of $\mathbf{T}_I$. The coordinate y^* separates the definition domains of $\mathbf{T}_{CF}$ and $\mathbf{T}_I$. The y_c is the coordinate of the maximum of the map $\mathbf{T}_{CF}$, and the coordinate $y_B = \hat{f}_B^{-1}(y_c)$ separates the domains Δ_0 and Δ_1 [see eq. (5.10)]. The construction of the points a, b, b', c, and d shows that the invariant set of the map $\mathbf{T}_{CF}$ is uncountable by Theorem 5.1. (b) Return time function under the same conditions as before. T_B is the return time at the coordinate y_B and separates the return times of cool flame peaks of type 0 from those of type 1. T_p is the return time during $\mathbf{T}_{CF}$ of the reinjection point of $\mathbf{T}_I$. At the right of y^* is the return time during $\mathbf{T}_I$ alone. (c) The unstable manifold W_u of the basic cycle under the same conditions as before in the (x, y) plane. The y (resp. x) axis is tangent to the unstable (resp. stable) manifold of the basic cycle crossing the section plane at $x = y = 0$. The point P_I is the reinjection point by the map $\mathbf{T}_I$. (d) Schematic representation of the Smale horseshoe under the same conditions as before in the (x, y) plane. Δ_0, Δ_1, and Δ_I are the three definition domains of the mappings of symbols 0, 1, and I. The line L is the preimage of the line Im L which cuts $\mathbf{T}_{CF}(\Delta_0 \cup \Delta_1)$ in the domain Δ_I near the maximum of the horseshoe. The line separating Δ_0 and Δ_1 is the preimage of the intersection of the line L with $\mathbf{T}_{CF}(\Delta_0 \cup \Delta_1)$.

b

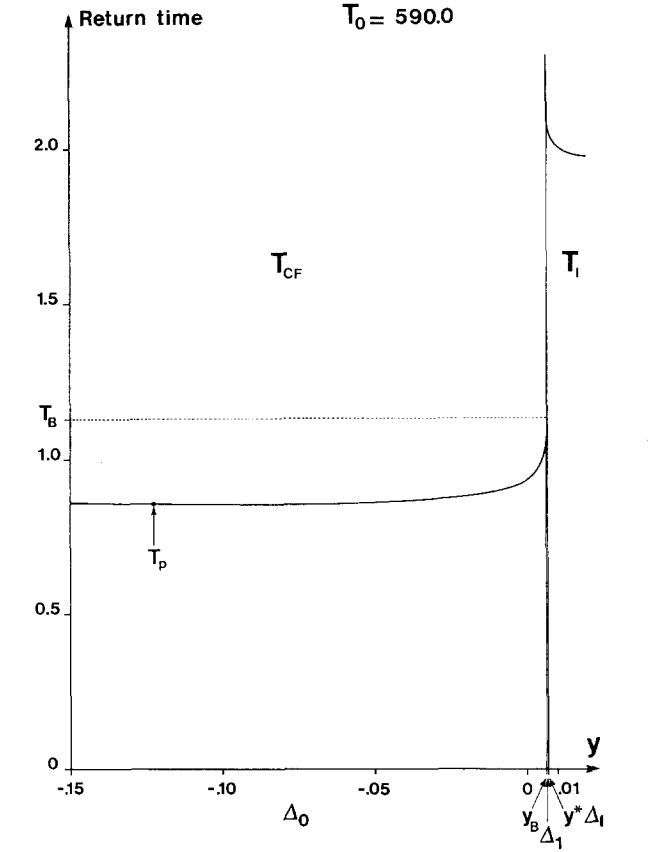

c

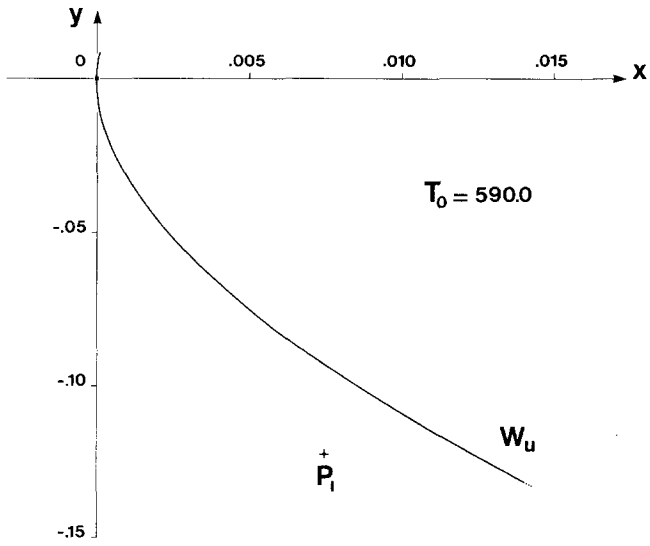

Fig. 17 (*continued*)

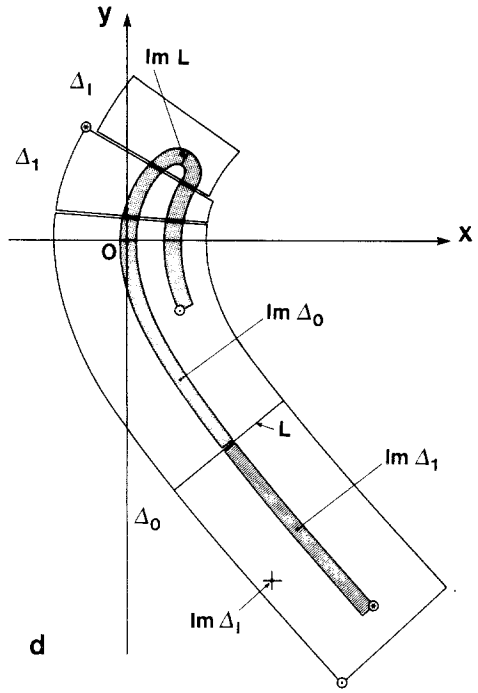

Fig. 17 (*continued*)

Figure 17c displays the geometry in the section plane (4.5) obtained numerically. The Smale horseshoe is quasi-one-dimensional confined near the unstable manifold W_u of the basic cycle C. It is represented schematically in Fig. 17d. The trajectories reaching the domain Δ_I will undergo ignition, which reinjects all the trajectories in a small pointlike domain denoted by Im Δ_I in Fig. 17d and P_I in Fig. 17c. The equations for $\mathbf{T}_I$ would thus be

$$\mathbf{T}_I \begin{cases} x' = x_I(T_0) \\ y' = y_I(T_0) \\ t' = t + \tau_I(y, x; T_0) \end{cases} \qquad \begin{matrix} (x, y) \in \Delta_I \\ (x_I, y_I) \in \Delta_0 \cup \Delta_1 \end{matrix} \tag{5.2}$$

Transversely, the Smale horseshoe is strongly contractive. [See the value of the stable eigenvalue λ_s of the basic cycle C in Eq. (4.2).] So the image of P_I by $\mathbf{T}_{CF}$ is quasi on the unstable manifold W_u as well as its next iterations by $\mathbf{T}_{CF}$. If W_u has the equation

$$W_u : x = w(y; T_0) \tag{5.3}$$

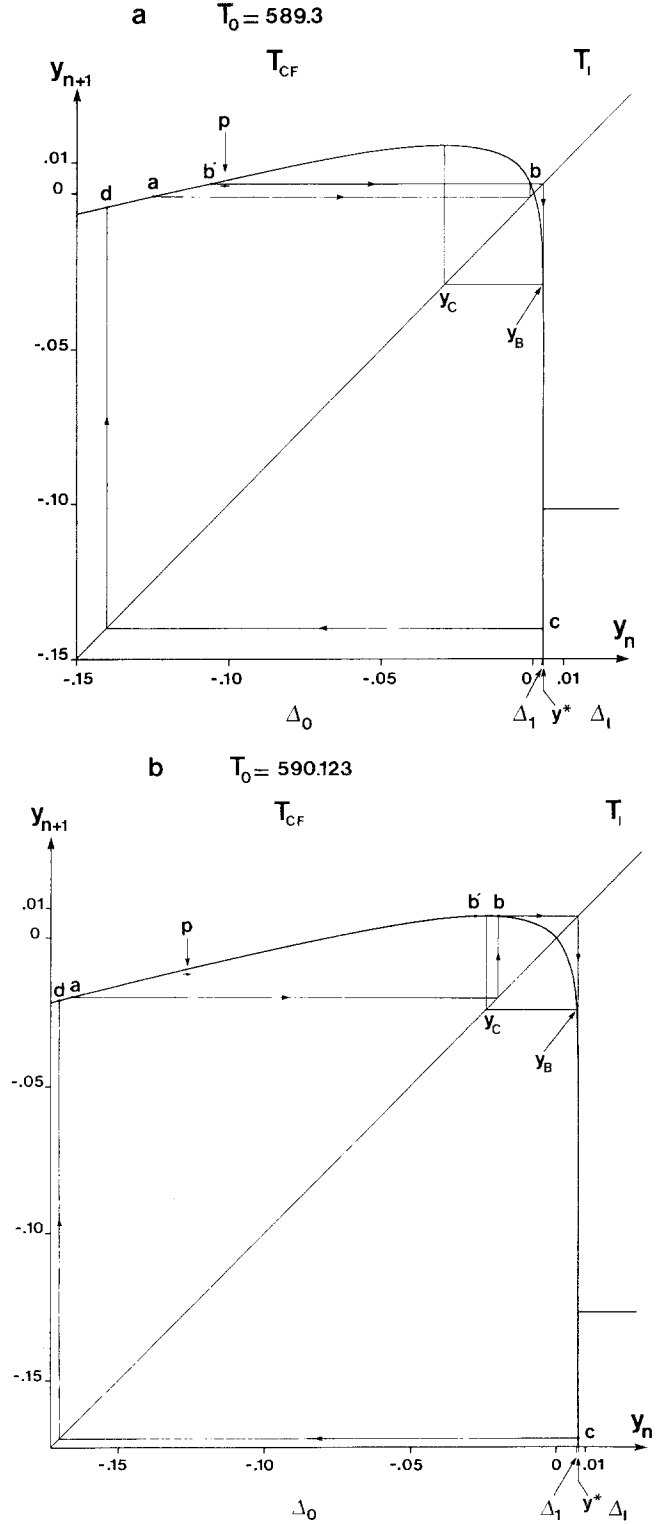

Fig. 18. Return mappings in the section plane $X = 0.022$ at (a) the ambient temperature $T_0 = 589.3$ and (b) $T_0 = 590.123$. The same notations are used as in Fig. 17a.

then the cool flame subdynamics may be approximated to a very good precision by the restriction of the 2D map $\mathbf{T}_{CF}$ to the unstable manifold W_u of the basic cycle C. More precisely, the system is reduced to a 1D map of the following form defined on an interval:

$$\mathbf{T}_{CF}: \quad y < y^* \quad \begin{cases} y' = F_{CF}(y, w(y)) = f(y) \\ t' = t + \tau_{CF}(y, w(y)) = t + \theta_{CF}(y) \end{cases} \tag{5.4}$$

$$\mathbf{T}_{CF} \circ \mathbf{T}_I: \quad y^* < y \quad \begin{cases} y' = F_{CF}(y_I, x_I) = p \\ t' = t + \tau_I(y, w(y)) + \tau_{CF}(y_I, x_I) = t + \theta_I(y) \end{cases} \tag{5.5}$$

with $p < y^*$, where we did not write explicitly the parameter dependence on T_0. Because P_I is away from W_u, its image by $\mathbf{T}_{CF}$ is away from the function $f(y)$ of $\mathbf{T}_{CF}$: it is represented by the point p in Figs. 17a, 18a, and 18b. The next iterations of the point p follow the 1D dynamics of $f(y)$ at the approximation of the figures. The complete dynamical system is the composition of the two maps given by Eqs. (5.4) and (5.5).

The transition between the regions IV and III at temperature $(T_0)_{III\text{-}IV}$ can be understood as the transition where the maximum of the 1D map $\mathbf{T}_{CF}$ at y_C of value $f(y_C)$ exceeds the threshold y^* that limits the definition domain of $\mathbf{T}_{CF}$. Above $(T_0)_{III\text{-}IV}$, the cool flame system $\mathbf{T}_{CF}$ remains attracting and is chaotic, as in Fig. 9b, because $f(y_C) < y^*$. Below $(T_0)_{III\text{-}IV}$, the top of $\mathbf{T}_{CF}$ exceeds the threshold y^* and ignition occurs repetitively after each escape from the hyperbolic repellor formed by the cool flame subdynamics of $\mathbf{T}_{CF}$. As observed in Figs. 17a and 18, the interval of escape between b' and b grows as the parameter T_0 decreases, so that escape is more and more important. In Fig. 18a at $T_0 = 589.3$, the dynamics is then governed principally by the linear behavior near the basic cycle C. This is why the low-ambient-temperature part of the bifurcation sequence of mixed-mode oscillations is explained in its main features by a linear map $\mathbf{T}_0$ rather than the nonlinear map $\mathbf{T}_{CF}$. The discrepancy between the prediction of the linear model with $\mathbf{T}_0$ and the numerical results in Fig. 12 noted in Section 4 is now understood as due to the remaining nonlinearity of the function $f(y)$ near the threshold y^*.

Let us now turn to the understanding of the bifurcation sequence of mixed-mode oscillations.

5.2. Piecewise Linear 1D Map Model

To illustrate the bifurcation phenomenon, we consider the following piecewise linear model

$$
\begin{aligned}
\mathbf{T}_{\mathrm{CF}}: \quad & y' = py, && 0 \leqslant y \leqslant 1/2 && \text{symbol 0} \\
& y' = p(1-y), && 1/2 < y \leqslant 1: && \text{symbol 1} \\
& \text{with} \quad p > 2 && && && (5.6) \\
\mathbf{T}_{\mathrm{I}}: \quad & y' = y_{\mathrm{I}} = \mu, && 1 < y: && \text{symbol I} \\
& \text{with} \quad 0 \leqslant \mu \leqslant 1
\end{aligned}
$$

The map is drawn in Fig. 19. The invariant set of the map $\mathbf{T}_{\mathrm{CF}}$ is described by a symbolic dynamics of alphabet $\{0, 1\}$. The coordinate $y[R]$ of the point

$$R = \omega_0\omega_1\omega_2\omega_3..., \qquad \text{with} \qquad \omega_i = 0 \text{ or } 1; \quad i = 0, 1, 2, 3,...$$

of the invariant set admits the following p-adic expansion:

$$y[R] = \omega_0 + \omega_1 \frac{(-)^{\omega_0}}{p} + \omega_2 \frac{(-)^{\omega_0+\omega_1}}{p^2} + \omega_3 \frac{(-)^{\omega_0+\omega_1+\omega_2}}{p^3} + \cdots \tag{5.7}$$

Because $p > 2$, the invariant set is a hyperbolic repellor of Cantor type characterized by a Hausdorff dimension $D = \ln 2/\ln p$ of zero Lebesgue

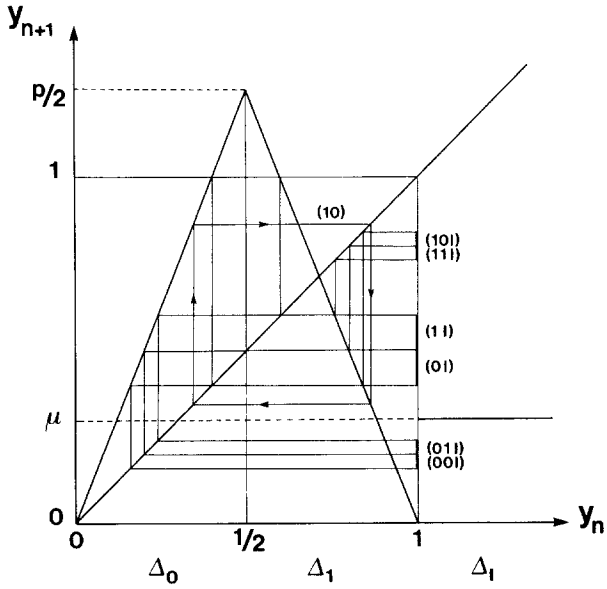

Fig. 19. The tentlike system of equations (5.6) with some periodic windows represented in the phase space.

measure on the interval [0, 1]. So almost all the points of the unit interval leave it after some iterations of $\mathbf{T}_{CF}$ to be mapped by $\mathbf{T}_I$ on $y=\mu$. Almost surely, μ is not a point of the Cantor set and the orbit is then periodic and superstable because $\mathbf{T}_I$ is pointlike. These periodic orbits are denoted $(\omega_1\omega_2\cdots\omega_n I)$, where the symbols ω_i take the values 0 or 1 according to the interval [0, 1/2] or]1/2, 1] visited in [0, 1]. The symbol I corresponds to a passage by $\mathbf{T}_I$. The bracket denotes the repetition of the symbolic pattern. Clearly, there exists a countable infinity of periodic windows corresponding to these superstable mixed-mode periodic orbits.

The bifurcations between these periodic orbits occur when μ reaches a point $y[R]$ of the Cantor set. The complete description of the bifurcations of the periodic attractors is easy in this particular model. Consider the set of all the finite sequences S of symbols 0 and 1 with the null sequence ϕ composed of no symbol. If $S=\omega_0\omega_1\cdots\omega_l$, let us define the parity of S as the parity of $\sum_{i=0}^{l}\omega_i$ and ϕ has the even parity. Equation (5.7) implies that

$$y[S010^\infty] < y[S110^\infty] \qquad \text{if } S \text{ is even}$$

$$y[S110^\infty] < y[S010^\infty] \qquad \text{if } S \text{ is odd}$$

Consequently, with the notation

$$m_S = (y[S010^\infty] + y[S110^\infty])/2$$

by following the preimages of the interval $(1/p, 1-1/p)$, we obtain the periodic windows as follows:

If S is even,

$$(S0I) \in (y[S010^\infty], m_S]$$

$$(S1I) \in (m_S, y[S110^\infty])$$

If S is odd,

$$(S1I) \in (y[S110^\infty], m_S)$$

$$(S0I) \in (m_S, y[S010^\infty])$$

where the intervals belong to the μ-parameter space. If the map $\mathbf{T}_{CF}$ (resp. $\mathbf{T}_I$) has a return time τ_{CF} (resp. τ_I), the period of (RI) is

$$l\tau_{CF} + \tau_I$$

if l is the length of the finite sequence R. From (5.7), the periodic window of this orbit has a width

$$\frac{1}{p^{l-1}}\left(\frac{1}{2}-\frac{1}{p}\right)$$

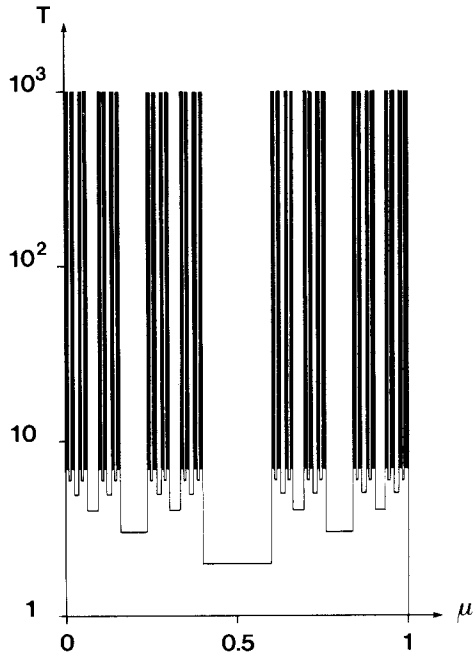

Fig. 20. Bifurcation diagram of the periodic attractors of the dynamical system (5.6) with the parameter $p = 2.5$, $\tau_{CF} = 1$, and $\tau_I = 1$. The period T versus the parameter value μ is drawn on a logarithmic scale. The Cantor set of the bifurcation parameter values appears from the vertical asymptotes of the diagram.

in the μ-parameter space. Figure 20 depicts the bifurcation diagram of the period versus the parameter.

There exists an infinite number of homoclinic tangencies toward which a sequence of periodic windows of increasing period accumulates. If IR is the homoclinic tangency occurring at $y[R]$ and if $[R]_l$ denotes the finite sequence containing the l first symbols of the infinite sequence R, then the window of the periodic orbit $([R]_l I)$ is in a neighborhood of $y[R]$ of diameter of order p^{-l} and on the side of $y[R]$ determinated according to the parity of $[R]_{l-1}$.

Furthermore, a countable set of homoclinic tangencies may be associated to a single periodic orbit of the basic invariant set. Let P and S be two finite sequences of 0 and 1; then all the homoclinic tangencies ISP^∞ are associated to the same periodic orbit (P), but occur at different parameter values given by $y[SP^\infty]$. The sequence of periodic windows accumulating at a homoclinic tangency ISP^∞ is less observable as the period l of (P) increases, because the rate of accumulation goes like $1/p^l$.

The homoclinic tangencies are uncountable and lie among the countable set of periodic windows. These results illustrate the complexity of the bifurcations of mixed-mode periodic attractors in such systems.

5.3. The Cantor-Like Hyperbolic Repellor of the Cool Flame Subdynamics

We now show that the invariant set of the cool flame subdynamics of the thermokinetic model (3.1)–(3.8) is of the Cantor type, like the preceding piecewise linear model. The answer is provided by a theorem of Li and Yorke,[31] which can be generalized to our case.

Consider the function $f(y)$ of the map $\mathbf{T}_{CF}$ given by Eq. (5.4) and Figs. 17a and 18. y_C denotes the coordinate of the maximum of $f(y)$. We define f_A on $y < y_C$ as the part of f that is strictly increasing, and f_B on $y_C \leqslant y < y^*$ as the part of f that is strictly decreasing, and then the intervals $\mathscr{I}_A$ and $\mathscr{I}_B$ by

$$\mathscr{I}_A = \{ y \in \mathscr{I} : y < f_A^{-1}(y^*) \}$$
$$\mathscr{I}_B = \{ y \in \mathscr{I} : f_B^{-1}(y^*) < y < y^* \}$$

In Figs. 17a, 18a, and 18b we construct the points a, b, b', c, and d such that the assumptions of the following theorem are satisfied.

Theorem 5.1. Let the function $f(y)$ be continuous on the intervals $\mathscr{I}_A$ and $\mathscr{I}_B$. Suppose there exist a point a such that $b = f(a)$, $c = f^2(a)$, and $d = f^3(a)$ and a point b' such that $c = f(b')$, with $a, b', d \in \mathscr{I}_A$ and $b, c \in \mathscr{I}_B$, and which satisfy

$$d \leqslant a < b' < b < c$$

Then f has an uncountable invariant set $\hat{\Lambda} \in \mathscr{I}_A \cup \mathscr{I}_B$.

We refer the reader to the paper of Li and Yorke for a proof of this theorem.[31] Let us remark that the uncountable set $\hat{\Lambda}$ of the theorem of Li and Yorke does not contain all the trajectories of the maximal invariant set Λ of $\mathbf{T}_{CF}$, but the theorem implies that the maximal invariant set Λ between the points d and c, which contains $\hat{\Lambda}$, is uncountable and of Cantor type.

Furthermore, we remark that $|f'|^{-1/2}$ is convex, so that the Schwarzian derivative of f is negative on $y < y^*$:

$$S(f)(y) = \frac{f'''(y)}{f'(y)} - \frac{3}{2}\left(\frac{f''(y)}{f'(y)}\right)^2 < 0 \tag{5.8}$$

Since the maximum $f(y_C)$ exceeds the upper boundary y^* of the definition domain of y, this property implies that the map f is hyperbolic on its invariant Cantor set Λ in the following sense. There exist a $K>0$ and a $\tau>1$ such that

$$|(f^n)'(y)| > K\tau^n \tag{5.9}$$

for all $n \geqslant 0$ and for all $y \in \Lambda$, as proved by van Strien.[36] As a consequence, the invariant Cantor set Λ is structurally stable and does not undergo bifurcations. It thus forms a hyperbolic repellor.

The invariant set Λ can be described by a symbolic dynamics in the following way. We partition the phase space below y^* into two domains,

$$\begin{aligned} \Lambda_0 &= \{ y \in \mathscr{I} : y < f_B^{-1}(y_C) \} \\ \Lambda_1 &= \{ y \in \mathscr{I} : f_B^{-1}(y_C) < y < y^* \} \end{aligned} \tag{5.10}$$

This particular choice is due to two reasons.

On one hand the difference between thin (symbol 0) and thick (symbol 1) cool flame peaks occurs in the return time of the map $\mathbf{T}_{CF}$ displayed in Fig. 17b. The return time sharply increases only near y^* for $y < y^*$, so that even the basic cycle at $y=0$ appears as a thin cool flame peak. Our choice corresponds to a partition of the return time at the time T_B in Fig. 17b.[5]

On the other hand, due to the particular shape of the map $\mathbf{T}_{CF}$, it does not have a second fixed point like the tentlike map $\mathbf{T}_{CF}$ of Section 5.2 (see Fig. 19). This feature is taken into account if we impose on the symbolic dynamics the condition that the symbol 1 is always followed by the symbol 0 and if we limit our symbolic description to the trajectories of the invariant set Λ contained between d and c.

Moreover, the following result holds concerning the order in which the points of Λ occur on the interval $y < y^*$. We define[37]

$$\theta_n(y) = \begin{cases} +1 & \text{if } f^{n+1} \text{ preserves the orientation near } y \\ -1 & \text{if } f^{n+1} \text{ reverses the orientation near } y \end{cases}$$

If the sequences $\boldsymbol{\theta}(y) = \{\theta_n(y)\}_{n=0}^{\infty}$ are ordered lexicographically, then we have the following result.[37]

[5] The form of the return time functions of $\mathbf{T}_{CF}$ and $\mathbf{T}_I$ is at the origin of the sharp increase of the period near the boundaries of the periodic windows observed in Section 4 (see Figs. 11, 12, and 15).

Proposition 5.2. If $y < y'$ $(< y^*)$, then $\theta(y) \geqslant \theta(y')$.

This proposition proves that the order of the points of Λ on the interval $\mathscr{I}$ is universal for the 1D iterations $f(y)$, i.e., identical for all the values of the parameter T_0 in Figs. 17a and 18. The order of the invariant set Λ is governed by a p-adic expansion similar to Eq. (5.7) if the symbolic dynamics is correctly identified.

According to the work of Mira, Holmes, and others,[37-39] we expect that the order of the stable manifolds of the invariant set of the 2D map $\mathbf{T}_{CF}$ of Eqs. (5.1), which is only quasi-1D, is close to the order of the invariant set of the 1D mapping $f(y)$. But there exists a scale where the 1D universal order breaks.[37-39] This scale is finer if the map $\mathbf{T}_{CF}$ is closer to a 1D mapping. However, we expect that the hyperbolicity of the invariant set will persist for the 2D map $\mathbf{T}_{CF}$.

Numerical computation reveals that the function $f(y)$ and the return time have a vertical asymptote at $y = y^*$ (see Figs. 17a and 17b). This mechanism is unknown to us, so that the function $f(y)$ is undefined in a very small domain

$$y^* - \Delta y \leqslant y \leqslant y^* + \Delta y$$

with $|\Delta y| < 6 \times 10^{-8}$ for all T_0. As a consequence, our knowledge of the bifurcation sequence is limited. With the given precision, the width of the largest undefined window in the T_0-parameter space is of order 10^{-5}. The unknown fraction of the T_0-parameter space is then of order 10^{-4}.

5.4. Bifurcation Sequence of Mixed-Mode Oscillations

We come back to the complete dynamical system composed of both $\mathbf{T}_{CF}$ and $\mathbf{T}_I$. We add to the partition (5.10) into Δ_0 and Δ_1 the following domain

$$\Delta_I = \{ y \in \mathscr{I} : y^* < y \} \tag{5.11}$$

A symbol of the alphabet $\{0, 1, I\}$ is assigned to the trajectory at a passage via the corresponding domain $\{\Delta_0, \Delta_1, \Delta_I\}$. The transition matrix of the symbolic dynamics is then the following (see Figs. 17a and 18):

$$\begin{array}{c} \\ 0 \\ 1 \\ I \end{array} \begin{array}{c} \begin{array}{ccc} 0 & 1 & I \end{array} \\ \begin{bmatrix} 1 & 1 & 1 \\ 1 & 0 & 0 \\ 1 & 0 & 0 \end{bmatrix} \end{array} \tag{5.12}$$

Thus, the stable trajectories of the system are superstable periodic orbits. They are classified according to their type (IR), where R is a finite sequence of 0 and 1 compatible with (5.12). The type of the periodic windows we observed in the thermokinetic model is presented in the last column in Table III.

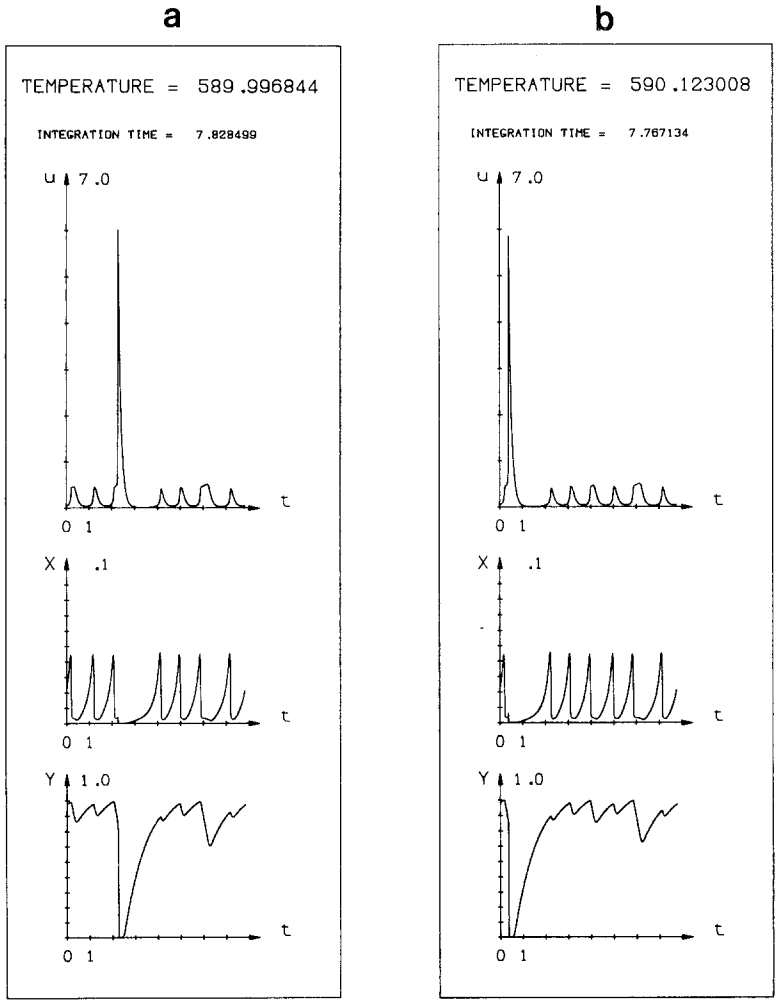

Fig. 21. (a) The homoclinic orbit of the homoclinic tangency occurring at $T_0 = 589.996844$ of type $I0^2 1 0^\infty$, computed from initial condition $x_0^* = 0$, $y_0^* = 0.005$ up to $x_1^* = 12 \times 10^{-7}$, $y_1^* < 2 \times 10^{-7}$ in the local coordinates (x, y) of the section plane $X = 0.022$. (b) Another homoclinic orbit at $T_0 = 590.123008$ of type $I0^4 1 0^\infty$, computed from initial condition $x_0^* = 0$, $y_0^* = 0.0094$ up to $x_1^* = 10^{-6}$, $y_1^* < 2 \times 10^{-7}$.

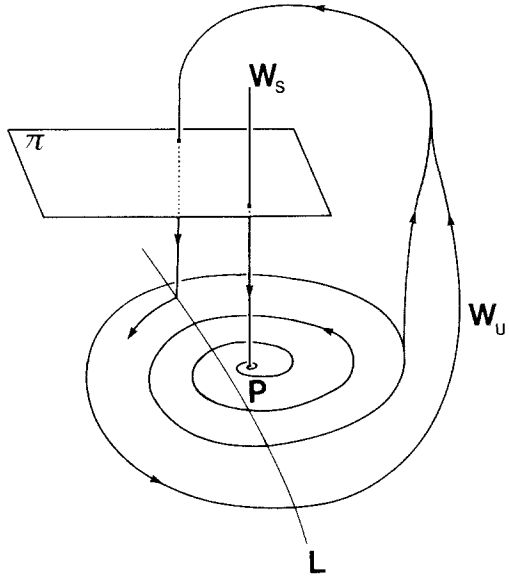

Fig. 22. Geometry of the reinjection mechanism to a saddle-focus fixed point of eigenvalues $(\rho \pm i\omega, \lambda)$, $|\rho/\lambda| < 1$, in the strongly contractive case. L is the line of the reinjection points on the two-dimensional unstable manifold as the parameter is varied.

As predicted by the homoclinic tangency to a Cantor-like invariant set, several homoclinic tangencies to the basic cycle C are expected to be embedded in the bifurcation sequence (see Section 5.2). Two such examples are shown in Fig. 21. Table IV summarizes the homoclinic tangencies we have observed in the thermokinetic model, either by direct numerical computation as those of Figs. 14, 16, and 21, or by inspection of Table III. Homoclinic tangencies to other, more complicated cycles of the invariant set have not been observed, for the following reason.

According to Eq. (2.19), the width of their periodic windows shrinks like $(\tilde{\lambda}_u)^{-2n}$, where $\tilde{\lambda}_u$ is the unstable eigenvalue of the corresponding basic

Table IV. The Observed Homoclinic Tangencies of the Thermokinetic Model of Pressure near 553 mm Hg[a]

$589.459801925 \pm 15 \times 10^{-9}$	$10I0^{\infty}$
$589.459801925 \pm 15 \times 10^{-9}$	10^3I0^{∞} (or $1010I0^{\infty}$)
$589.996843934 \pm 3 \times 10^{-7}$	$I0^210^{\infty}$
$589.99750532 \pm 1 \times 10^{-8}$	$I0^210^510^{\infty}$
$590.12300821 \pm 2 \times 10^{-7}$	$I0^410^{\infty}$ (or $I0^21010^{\infty}$)

[a] All are associated to the basic cool flame cycle.

cycle. Since all the cycles different from the fixed point $y=0$ of $\mathbf{T}_{CF}$ have necessarily a passage via the domain Δ_1 where the slope is very large, so is $\tilde{\lambda}_u$ and the corresponding periodic windows are extremely small.

The order of the periodic windows in the bifurcation sequence depends on the relative shift of the reinjection point p of $\mathbf{T}_{CF} \circ \mathbf{T}_I$ with respect to the invariant set Λ of $\mathbf{T}_{CF}$. We observe in Figs. 17a and 18 that the point p is always contained between the points $b=f(a)$ and $c=f(b)$ on the y axis. As the parameter T_0 increases, the point p decreases and then increases with respect to the points b and c, as seen in figs. 17a and 18. The order of the periodic windows is thus a complicated function. The exact knowledge of the relative shift of p with respect to the invariant set Λ would explain in detail the order of the bifurcation sequence. However, we are confronted by practical limits because the thermokinetic model we studied is a 3D stiff differential equation system. Nevertheless, the observation of a horseshoe in the cool flame subdynamics with a homoclinic tangency due to the ignition subdynamics already gives an understanding of the origin of complexity in the bifurcation sequence as well as its organization rules.

6. CONCLUSIONS

We have seen that homoclinicity is important to an understanding of the bifurcation sequences of mixed-mode oscillations as well as chaotic behaviors. The concept of homoclinic orbit provides a classification of the various bifurcation sequences according to the properties of the basic hyperbolic invariant set: a fixed point, a limit cycle, a torus, a quasirandom set. Furthermore, generalizations to higher dimensions are possible.

Let us comment on the disappearance of chaotic behaviors in the region III below the scale 10^{-7} in the phase space. As discussed in Section 2, the reason is that the dynamics in the phase space is strongly contractive with a passage through a quasipointlike region, when ignition occurs. This is not the case in the cool flame regime, where chaos does exist and in fact provides the basic invariant set to which homoclinic tangencies are realized. The Belousov–Zhabotinskii reaction does not have the very stiff dependence on the temperature as in a thermokinetic combustion system and is thus more likely to sustain chaotic behaviors as revealed by experiments or in models.

Some comments are now in order on the comparison of the bifurcation sequence of this thermokinetic model to those revealed by experiments on acetaldehyde combustion, where a sequence $\{P_1, P_2, P_3, P_4, P_5\}$ in simple order has been observed and where the existence domain of the mixed-mode oscillations is larger than in the thermokinetic model (3.1)–(3.5).[6,7] In a three-variable model, such a sequence

could be generated by a homoclinic tangency to a periodic orbit with both Liapunov numbers λ_u, λ_s positive. However, we believe that this possibility has to be excluded. Indeed, the branch of the cool flame oscillations can become unstable and acquire a positive Liapunov number λ_u only by a tangent bifurcation in three-dimensional systems. But the branch would be folded with a low-temperature bound and no mixed-mode oscillation would exist below the low-temperature boundary of the cool flame oscillations, in contradiction with the observations. This incompatibility would no longer exist in a four-variable model, with three Liapunov numbers $\lambda_s \lambda_{u_1} \lambda_{u_2} > 0$ such that $|\lambda_s| < 1 < |\lambda_{u_1}| < |\lambda_{u_2}|$ and $|\lambda_s \lambda_{u_1}| < 1$ with $\lambda_{u_1} > 0$. It is known that the Liapunov numbers relevant to the dynamics near the homoclinic orbit are always those close to the unit circle.

Nevertheless, there remains another possibility within a three-variable model. Type I sequences of mixed-mode oscillations may be mimicked by a reinjection mechanism to a saddle-focus fixed point of eigenvalues $(\rho \pm i\omega, \lambda)$ satisfying the Shil'nikov condition $|\rho/\lambda| < 1$. In the general case, this mechanism would lead to a homoclinic orbit to the fixed point.[15] But, since the flow near the reinjection loop is very strongly contractive, the unstable manifold will be virtually one-dimensional when it is reinjected back to the fixed point. By varying one parameter, the unstable manifold will then pass in the vicinity of the stable manifold without being able to include it to form a homoclinic orbit. Therefore, an incomplete bifurcation sequence of mixed-mode oscillations of the type $\{P_1, P_2, ..., P_{n-1}, P_n, P_{n-1}, ..., P_2, P_1\}$ with finite n can be generated (see Fig. 22). This type of incomplete bifurcation sequence and the sequence of type II discussed in Section 2 might both be realized in a single model; a transition between the two could also occur when the parameters change. In our simulations with pressure near 553 mm Hg, the eigenvalues of the fixed point do not satisfy the Shil'nikov condition, so that the complete type II sequence is realized rather than the incomplete type I sequence.

The bifurcation sequences of type II should occur very naturally in real systems, since they are directly connected to the period doubling way of destabilizing the basic periodic orbit, which is quite generic. Therefore, this particular bifurcation sequence of mixed-mode periodic solutions predicted by the model (3.1)–(3.8), together with the period doubling sequence of the basic, cool-flame limit cycle, are expected to be found experimentally in hydrocarbon oxidation systems.

To conclude, we can say that the homoclinic systems provide a general classification scheme of the universal behaviors of chemical systems far from equilibrium, while maintaining the relation between the abstract 1D or 2D mappings and the underlying differential equations for the physicochemical state variables.

ACKNOWLEDGMENTS

It is our pleasure to thank Prof. G. Nicolis for encouragement and support in this research, as well as for reading and improving our manuscript. We also thank Dr. J. Griffiths for useful discussions and comments on the manuscript. X.-J. W. wishes to express his gratitude to Prof. C. Y. Mou for inspiring discussions. P. G. is Aspirant at the National Fund for Scientific Research (Belgium) and would like to thank Dr. C. Sparrow for a fruitful exposition of his method of locating periodic orbits. This work was partly supported by the U. S. Department of Energy under contract DE-AS05-81ER10947.

REFERENCES

1. J.-C. Roux, *Physica* **7D**:57 (1983), and references therein.
2. J. S. Turner, J.-C. Roux, W. D. McCormick, and H. L. Swinney, *Phys. Lett.* **85A**:9 (1981).
3. C. Vidal, Dynamic instabilities observed in the Belousov–Zhabotinsky system, in *Chaos and Order in Nature*, H. Haken, ed. (Springer, Berlin, 1981), pp. 69–82.
4. J. L. Hudson, M. Hart, and D. Marinko, *J. Chem. Phys.* **71**:1601 (1979).
5. M. Orban and I. R. Epstein, *J. Phys. Chem.* **86**:3907 (1982).
6. P. Gray, J. F. Griffiths, S. M. Hasko, and P. G. Lignola, *Combustion Flame* **43**:175 (1981); *Proc. R. Soc. Lond. A* **374**:313 (1981).
7. X.-J. Wang and C. Y. Mou, *J. Chem. Phys.* **83**:4554 (1985).
8. R. H. Simoyi, A. Wolf, and H. L. Swinney, *Phys. Rev. Lett.* **49**:245 (1982).
9. A. S. Pikovsky, *Phys. Lett.* **85A**:13 (1981).
10. R. A. Schmitz, G. T. Renola, and P. C. Garrigan, *Ann. N. Y. Acad. Sci.* **316**:638 (1979).
11. O. E. Rössler, *Z. Naturforsch.* **31a**:259 (1976).
12. O. E. Rössler, Chaos, in *Structural Stability in Physics*, W. Güttinger and H. Eikemeier, eds. (Springer, Berlin, 1979), pp. 290–309.
13. A. Arnéodo, P. Coullet, and C. Tresser, *J. Stat. Phys.* **27**:171 (1982).
14. C. Tresser, *Ann. Inst. Henri Poincaré Phys. Theor.* **40**:441 (1984).
15. P. Gaspard and G. Nicolis, *J. Stat. Phys.* **31**:499 (1983).
16. P. Glendinning and C. Sparrow, *J. Stat. Phys.* **35**:645 (1984).
17. P. Gaspard, R. Kapral, and G. Nicolis, *J. Stat. Phys.* **35**:697 (1984).
18. P. Gaspard, Periodic and nonperiodic dynamical behaviors near homoclinic systems, in *Fluctuations and Sensitivity in Nonequilibrium Systems*, W. Horsthemke and D. K. Kondepudi, eds. (Springer, Berlin, 1984), p. 265.
19. F. Argoul, A. Arnéodo, and P. Richetti, Experimental evidence of homoclinic chaos in the Belousov–Zhabotinskii reaction, *Phys. Lett.* **120A**:269 (1987).
20. J. Neimark and L. Shil'nikov, *Sov. Math. Dokl.* **6**:305 (1965); L. Shil'nikov, *Sov. Math. Dokl.* **6**:163 (1965); *Mat. Sb.* **10**:91 (1970).
21. Y. Pomeau and P. Manneville, *Commun. Math. Phys.* **74**:189 (1980).
22. N. K. Gavrilov and L. P. Shil'nikov, *Mat. SSSR Sb.* **17**:467 (1972); **19**:139 (1973).
23. J. Guckenheimer and P. Holmes, *Nonlinear Oscillations, Dynamical Systems and Bifurcations of Vector Field* (Springer, New York, 1983).
24. S. Smale, Differentiable dynamical systems, in *The Mathematics of Time* (Springer, New York, 1980), pp. 1–82.
25. P. Gaspard, *Phys. Lett.* **97A**:1 (1983).

26. C. Sparrow, *The Lorenz Equations: Bifurcations, Chaos, and Strange Attractors* (Springer, New York, 1982), Appendix E.
27. Ya. G. Sinai and E. B. Vul, *J. Stat. Phys.* **23**:27 (1980).
28. S. De Gregorio, *J. Stat. Phys.* **38**:947 (1985).
29. Subroutine D02EBF, NAG Fortran Library, Numerical Algorithms Group, Oxford and Illinois (1983).
30. M. J. Feigenbaum, *J. Stat. Phys.* **19**:25 (1978); **21**:669 (1979).
31. T.-Y. Li and J. A. Yorke, *Am. Math. Mon.* **82**:985 (1975).
32. P. Gray, J. F. Griffiths, and S. M. Hasko, *Proc. R. Soc. Lond. A* **396**:227 (1984).
33. S. Newhouse, *Topology* **12**:9 (1974); *Publ. Math. IHES* **50**:101–152 (1979).
34. C. Robinson, *Commun. Math. Phys.* **90**:433 (1983).
35. P. Hartman, *Ordinary Differential Equations* (Wiley, New York, 1964).
36. S. J. van Strien, On the bifurcation creating horseshoes, in *Dynamical Systems and Turbulence*, D. A. Rand and L. S. Young, eds. (Lecture Notes in Mathematics 898, Springer, Berlin, 1981), pp. 316–351.
37. P. Holmes and R. F. Williams, *Arch. Rat. Mech. Anal.* **90**:115 (1985).
38. D. Fournier, H. Kawakami, and C. Mira, *C. R. Acad. Sci. Paris I* **298**(11):253 (1984).
39. P. J. Holmes, *Phys. Lett.* **104A**:299 (1984).
40. J. H. Curry and J. R. Johnson, *Phys. Lett.* **92A**:217 (1982).
41. X.-J. Wang, Homoclinic tangency to a Smale horseshoe, preprint (1987).